Atmos. Chem. Phys. Discuss., 14, 28609–28655, 2014
www.atmos-chem-phys-discuss.net/14/28609/2014/
doi:10.5194/acpd-14-28609-2014

Atmospheric Chemistry and Physics Discussions

The impacts of fireworks burning at Chinese Spring Festival on air quality and human health: insights of tracers, source evolution and aging processes

S. Kong[1,2], L. Li[2], X. Li[2], Y. Yin[1,2], K. Chen[1,2], D. Liu[4], L. Yuan[2], Y. Zhang[2], Y. Shan[2], and Y. Ji[3]

[1]Collaborative Innovation Center on Forecast and Evaluation of Meteorological Disasters, Nanjing University of Information Science and Technology, Nanjing, 210044, China
[2]Key Laboratory for Aerosol-Cloud-Precipitation of China Meteorological Administration, School of Atmospheric Physics, Nanjing University of Information Science & Technology, Nanjing 210044, China
[3]Colloge of Environemental Science and Engineering, Nankai University, Tianjin, 100086, China
[4]School of Earth, Atmospheric and Environmental Science, University of Manchester, Manchester, UK

Received: 1 October 2014 – Accepted: 27 October 2014 – Published: 19 November 2014

Correspondence to: Y. Yin (yinyan@nuist.edu.cn); Y. Q. Ji (jiyaqin@nankai.edu.cn) and S. F. Kong (kongshaofei@126.com)

Published by Copernicus Publications on behalf of the European Geosciences Union.

ACPD
14, 28609–28655, 2014

Abstract

To understand the impact of fireworks burning (FW) particles on air quality and human health during winter haze period, thirty-nine elements, ten water-soluble ions and eight fractions of carbonaceous species in atmospheric $PM_{2.5}$ at Nanjing were investigated during 2014 Chinese Spring Festival (SF). Serious regional haze pollution persisted throughout the entire sampling period, $PM_{2.5}$ averaging at $113 \pm 69\,\mu g\,m^{-3}$ and visibility at 4.8 ± 3.2 km. The holiday effect led to almost all the chemical species decreasing during the SF, except for Al, K, Ba and Sr which were related to FW. The source contributions of coal combustion, vehicle emission and road dust descreased dramatically, whereas FW contributed to about half of the $PM_{2.5}$ during SF period. The intensive emission of FW particles at New Year's Eve accounted for 60.1 % of the $PM_{2.5}$. They also significnatly modified the chemical compositions of $PM_{2.5}$, with 39.3 % contributed by increased organic matter, followed by steadly increased loadings of secondary inorganic ions. The aging processes of the FW particles lasted for at least six days reflected by the variation of SO_4^{2-}, characterized by heterogeneous reactions of SO_2 and NO_x on crustal materials directly from FW, the replacement of Cl^- by NO_3^- and SO_4^{2-}, coating of NO_3^- and SO_4^{2-} on soot, formation of secondary organic aerosols and metal-catalyzed formation of NO_3^- and SO_4^{2-} at higher relative humidity. During aging, the main contributors to the extinction coefficient shifted from elemental carbon and organic matter to sulfate ammonium. The particles raised higher cancer risks by heavy metals (especially for Cd and As) as 1.62×10^{-6}. This study provided detailed composition data and first comprehensive analysis of the aging processes of FW particles at serious haze pollution period and their potential impact on human health.

1 Introduction

Atmospheric pollutants emitted from fireworks burning (FW) at festivals or special celebration events around the world have recently received wide attention, such as Guy

ACPD
14, 28609–28655, 2014

Fawkes' night at UK (Allan et al., 2010; Godri et al., 2010), Pyronale® 2009 and Pyromusikale® (Dutschke et al., 2011), Montréal International Fireworks competition (Joly et al., 2010), New Year's celebrations (Zhang et al., 2010; Do et al., 2012; Feng et al., 2012; Jiang et al., 2014; Jing et al., 2014; Tian et al., 2014; Ye et al., 2014), Diwali (Godri et al., 2010), Las Fallas in Valencia (Moreno et al., 2007), new Millennium in Germany (Wehner et al., 2000), 2006 FIFA World Cup (Vecchi et al., 2008) and Lantern Festival (Do et al., 2012; Tsai et al., 2012). Besides the direct possible dangers like the exposure to sound pressures (Dutschke et al., 2011) or firework-related injuries (Do et al., 2012), their burning results in massive quantities of pollutants, leading to degradation of air quality (Wang et al., 2007; Sarkar et al., 2010; Dutschke et al., 2011; Do et al., 2012; Feng et al., 2012; Tsai et al., 2012; Jiang et al., 2014; Jing et al., 2014; Yang et al., 2014; Tian et al., 2014) and raising serious human health concerns (Godri et al., 2010; Do et al., 2012). Evidence suggests that inhalation of fumes containing high levels of specific elements such as chlorine can cause mucosal irritation and acute respiratory distress syndrome (Joly et al., 2010). A toxicity study reported that the samples collected in the post-FW period were more toxic than those in the pre-FW period according to the viabilities of BEAS-2B cells after 24 h incubation with the particle extracts (Do et al., 2012). A positive significant relationship was also found between particulate matter oxidative burden and individual trace metals associated with FW (Godri et al., 2010).

China is the largest firework producing country in the world (Tian et al., 2014). For the Chinese New Year day (CNY), in the Spring Festival (SF) at January or February of lunar Chinese calendar, high-profile FW events occurred at the midnight of the CNY's Eve in national scale, from small villages to megacities. It should be noted that FW events always occured in an already highly polluted urban air in China (Supplement S1). In winter, increased coal consumption for heating (Li and Zhang, 2014) and stable atmospheric conditions always raise serious haze pollution in central and eastern China. On January 2013, the whole central and eastern China was shrouded in a long-lasting severe haze episode (Wang et al., 2014). According to the Chinese Min-

ACPD
14, 28609–28655, 2014

istry of Environmental Protection, at 31 January 2014, about 80 % of 161 cities held average $PM_{2.5}$ concentrations higher than 150 $\mu g\,m^{-3}$ (Ye et al., 2014). The addition of pollutants from FW deteriorates ambient air quality during the SF and its impact can vary sigificantly with FW duration and meteorological conditions (Vecchi et al., 2008; Yu et al., 2013).

Previous studies have extensively characterized the physicochemical signatures of FW emissions, such as gaseous pollutants (Wehner et al., 2000; Attri et al., 2001; Wang et al., 2007; Vecchi et al., 2008; Tan et al., 2009; Godri et al., 2010), particle size distribution and number concentration (Wehner et al., 2000; Vecchi et al., 2008; Zhang et al., 2010; Dutschke et al., 2011; Yang et al., 2014), chemical components including trace elements (Wang et al., 2007; Moreno et al., 2007; Vecchi et al., 2008; Estrellan and Iino, 2010; Godri et al., 2010; Joly et al., 2010; Do et al., 2012; Tsai et al., 2012; Tian et al., 2014; Yang et al., 2014), organic carbon (OC) and elemental carbon (EC) (Estrellan and Iino, 2010; Tsai et al., 2012; Feng et al., 2012; Tian et al., 2014; Yang et al., 2014) and water-soluble ions (Wang et al., 2007, 2013; Vecchi et al., 2008; Shen et al., 2009; Estrellan and Iino, 2010; Tsai et al., 2012; Jiang et al., 2014; Tian et al., 2014; Yang et al., 2014). Recently, single particle's chemical compositions (Allan et al., 2010; Jiang et al., 2014), morphology and mixing properties (Li et al., 2013) and optical properties (Yu et al., 2013) of FW particles had been reported. However, there are to date still two shortages.

Firstly, no studies reported the chemical compositions (crustal elements, trace elements, water-soluble ions, OC and EC) of FW particles completely, considering the complex manufacture materials of FW (Supplement S2). Although Estrellan and Iino (2010), Feng et al. (2012), Yang et al. (2014) and Tian et al. (2014) reported the ions, elements and carbonaceous species synchronously, some important species were missed, such as Na, Mg, K, Ti, NH_4^+ and Cl^- in Tian et al. (2014), OC in Estrellan and Iino (2010), Si and some heavy elements in Feng et al. (2012) and crustal elements in Yang et al. (2014). These species are all highly elevated during FW events. Crustal elements including Na, Mg, Al, Si, K, Ca, Ti, Fe and Mn were always missing

ACPD
14, 28609–28655, 2014

or not sufficiently studied in FW particles. However, except for inorganic and organic chemicals such as charcoal, potassium nitrate, potassium chlorate, potassium perchlorate, sulfur, manganese, sodium oxalate, aluminum, iron powder, strontium nitrate, and barium nitrate (Shen et al., 2009; Jing et al., 2014), clay is also used to seal the top and bottom of fireworks as shown in Supplement S3. 90 % of the total mineral aerosol was from the emission of FW on the lantern night in Beijing (Wang et al., 2007). The incomplete compositions of FW particles may bias the identification of particle sources during FW period and limit our understanding of its aging processes. For example, crustal elements-Al, Si and Ca were thought to result from the resuspension of materials already deposited on the ground (caused by pyrotechnic device explosions) and hereby the resuspended dust was regarded as a contributor to atmospheric particles during SF (Tian et al., 2014). Without detecting the crustal and trace elements, secondary particulate matter accounted for 63–82 % of $PM_{1.0}$ during FW periods in Beijing (Jiang et al., 2014).

Secondly, all the former studies unanimously agreed with that FW contributed to elevated concentrations of particles and associated chemical species, but no studies concerned the aging processes of particles after emitted from intensive FW. The cocktail of primary pollutants released may exhibit varied interactions among themselves, and if aided by favourable atmospheric conditions, may lead to the formation of secondary pollutants (Sarkar et al., 2010). Do et al. (2012) pointed that the sub-micron aerosol or accumulation-mode particles from FW can suspend in the air for very long periods, from days to weeks, potentially causing pollution to large areas. Data in literature verified the exsitence of aging processes of FW particles, though it has not been discussed. For example, Li et al. (2013) indicated that emissions from FW significantly changed the transformation pathway from SO_2 to SO_4^{2-} and the FW particles can influence the air at downwind site (50 km far away). And after about two days, the elevated $PM_{2.5}$ mass concentrations at CNY's Eve decreased to the level of the day before CNY (pre-CNY). In Beijng, $PM_{2.5}$ mass concentrations at CNY's Eve decreased to the level of pre-CNY in one day, while secondary ions (SO_4^{2-}, NH_4^+ and NO_3^-) and organic mat-

ACPD
14, 28609–28655, 2014

ter (OM) increased first and then descreased to the level of pre-CNY after three days (Wang et al., 2007). In Jinan, a "tailing" phenomena was found, indicating that NH_4^+ and NO_3^- did not increase (peaking at 08:00 and 12:00 local time (LT), respectively) immediately with the concentrations of particles (peaking at 00:00 LT) after emitted at CNY's Eve (Yang et al., 2014). In Shanghai, NH_4^+ and NO_3^- also increased in the first day after emitted at CNY's Eve and then decreased to the level of pre-CNY in the third day and the decreasing rate of $PM_{2.5}$ was faster than that for OC (Feng et al., 2012). Therefore, we still need to answer the following questions: (1) are the decreasing trends of particles and associated chemical components the same? (2) How long and how far can FW influence the air quality at certain meteorological conditions? (3) During aging and transport, which type of chemical reactions will the FW particles undergo and how will specific chemical ratios vary?

Due to rapid economic expansion and urbanization, the occurrence frequency of haze has increased rapidly in recent 30 years at the Yangtze River Delta region (Wang et al., 2014). As one of the central megacities of this region, Nanjing is suffering from serious air pollution and the occurrence of hazy days increased from 1961 to 2005 (Kang et al., 2013). Thus, it provides a unique site and opportunity to study the chemical composition evolution and source variation during haze-clear days with the injection of intensive FW at SF. The main purpose of this study is to: (1) characterize in detail the chemical compositions of atmospheric $PM_{2.5}$ before, during and after intensive FW events; (2) identify how long and how much can the FW particles influence $PM_{2.5}$ by tracer analysis and receptor models; (3) emphasize how can the FW particles affect visibility and human cancer and non-cancer risks; (4) analyze the FW particle aging processes by specific species and ratios. The data and analysis will improve the knowledge of chemical compositions of FW particles, their evolution during serious haze pollution periods and their influence on visibility and human health.

ACPD
14, 28609–28655, 2014

2 Methodology

2.1 $PM_{2.5}$ collection

From 24 January to 21 February 2014, a sampling campaign of $PM_{2.5}$ was conducted on the rooftop (40 m high) of a building in Nanjing University of Information Science & Technology (Kang et al., 2013; Wang et al., 2014). It is a suburban site, surrounded by residential communities at the west, south, north and southeast directions. There is a steel factory 2 km to the east of the campus and a chemical industry park about 10 km to the northeast. It faced one road with heavy traffic, about 200 m in the east. Location of the sampling site was shown in Fig. 1 and Supplement S4. During the sampling period, CNY at 30 January and Lantern Festival (LF) at 14 Feburary were included. In CNY's and LF's Eve, numerous fireworks were consumed. The SF holiday was from 30 January to 7 February. $PM_{2.5}$ samples were collected for about 24 h using two medium-volume air samplers (TH-150C, Wuhan Tianhong Ltd., China) on quartz fiber filters (baked at 800 °C for 2 h) and polypropylene fiber filters (baked at 80 °C for 0.5 h) at a flow rate of 100 L min^{-1}. The hourly online $PM_{2.5}$ mass concentrations for the nine monitoring sites set by Jiangsu Environmental Monitoring Center were collected from the pubic platform (http://218.94.78.75/jsair/) (their locations can be found in Supplement S4). Twenty four pairs of filter samples were collected (Supplement S5). By using a microbalance (Ohaus Discovery DV214CD) with balance sensitivity as ±0.010 mg, filters were weighed before and after sampling under controlled environment with temperature and relative humidity (RH) of 22 °C and 35 %. Then they were stored at −20 °C until chemcial analysis. The quartz fiber filters were for analyzing water-soluble inorganic ions, OC and EC. Polypropylene fiber filters were for elemental analysis.

ACPD
14, 28609–28655, 2014

2.2 Chemical analysis

Inductively coupled plasma-mass spectroscopy (ICP-MS) (Agilent 7500a, Agilent Co. USA) was used for analyzing Li, Be, Na, Mg, Al, P, K, Ca, Sb, Sc, Ti, V, Cr, Mn, Co, Ni, Cu, Zn, As, Rb, Y, Mo, Cd, Sn, Cs, La, Ce, Sm, W, Tl, Pb, Bi, Th and U. Nine elements including Si, Al, Ca, Mg, Fe, Ti, Ba, Sr and Zr were analyzed by inductively coupled plasma-optical emission spectrometer (ICP-OES). Al, Ca, Mg and Ti were analyzed by both ICP-MS and ICP-OES, and results from the latter were used as the analysis accuracy for the four elements by ICP-OES was better than that by ICP-MS (Kong et al., 2014a). Ten ions including NH_4^+, Na^+, Mg^{2+}, K^+, Ca^{2+}, F^-, Cl^-, NO_2^-, NO_3^- and SO_4^{2-} were analyzed by a professional Ion Chromatograph (Wan Tong 850, Switzerland). DRI Model 2001 (Thermal/Optical Carbon Analyzer) with the IMPROVE thermal/optical reflectance protocol was used for OC and EC analysis (Han et al., 2008, 2010; Huang et al., 2012; Li et al., 2012; Wang et al., 2013; Kong et al., 2014a). A 0.188 cm^2 punch area from the quartz filter was heated to produce four OC fractions: OC1, OC2, OC3 and OC4 at temperatures of 120, 250, 450 and 550 °C in a non-oxidizing He atmosphere, three EC fractions: EC1, EC2 and EC3 at 550, 700 and 800 °C in an oxidizing atmosphere of 2 % O_2/98 % He and optically detected pyrolized carbon (OPC). OC is defined as OC1 + OC2 + OC3 + OC4 + OPC and EC is calculated by EC1 + EC2 + EC3-OPC. Char-EC is defined as EC1 minus OPC, and soot-EC is the sum of EC2 and EC3 (Han et al., 2008, 2010). The pre-treatment and chemical analysis procedures and quality assurance and control are described detailedly in our previous works (Li et al., 2012; Kong et al., 2014a, b; Li et al., 2014).

2.3 Meteorological parameters

The meteorological parameters including relative humidity (RH), visibility, wind speed, wind direction and temperature were recorded by the meteorological observatory of our university (http://qxt.nuist.edu.cn/). The rainfall information was obtained from http://www.wunderground.com/. According to China Meterological Administration, fog

ACPD
14, 28609–28655, 2014

is defined as visibility < 10 km and RH > 90 % and haze is defined as visibility < 10 km and RH < 80 %. For visibility < 10 km and 80 % < RH < 90 %, it is fog-haze mixing day. Figure 2 shows that the visibility is generally below 10 km (averaged as 4.8 ± 3.2 km), indicating fog, haze or fog-haze mixing events frequently occurred. At 4 February, a strong cold front passed through, leading to high visibility (14.7 km), low temperature (2.4 °C) and high wind speed (3.5 m s^{-1}). The wind speed remained mostly below 3 m s^{-1} (averaged as 2.2 ± 0.7 m s^{-1}), suggesting stagnant weather conditions.

2.4 Data processing

2.4.1 Back trajectory calculation

Three-day air mass back trajectories are calculated using NOAA Air Resource Lab HYSPLIT 4.8 model, driven by the GDAS meteorological dataset (1° × 1°) (Kong et al., 2014b). A 72 h back trajectory is adopted with the starting height of 500 m a.g.l. (Huang et al., 2012). Cluster analysis is adopted which results in sub-sets of trajectories with backward trajectories computed every six hour (00:00, 06:00, 12:00 and 18:00 LT) each day. The clustering process is described in detail in Hysplit User's Guide-Version 4. The mixing layer height is calculated every three hours each day by the NOAA's READY Archived Meteorology online calculating program (http://ready.arl.noaa.gov/READYamet.php). This program will produce a time-series of calculated boundary layer depth using the chosen meteorological data. As shown in Fig. 3, 43 % (cluster 3, 4 and 5) of the air masses origined from the Mongolia and crossed Chinese coastal seas; 31 % (cluster 1) was from the north China and transported across Shandong peninsula; 26 % (cluster 2) was from central China. Cluster 1 and cluster 2 transported for short distances, which may easily raise regional air pollution, as the Shandong peninsula and central and eastern China hold intensive anthropologic sources for air pollutants.

ACPD
14, 28609–28655, 2014

2.4.2 Principal component analysis

Principal component analysis (PCA) is used to identify the sources for particles at periods before (24–29 January), during (30 January–6 February), after SF holiday (12–21 February) and the whole period. It can analyze multivariate data sets structure and identify a smaller number of independent factors to explain the data variance. Factor loadings are related to the source emission compositions. A varimax normalized rotation is adopted by SPSS 13.0 software in this study (Kong et al., 2010).

2.4.3 Health risk assessment of heavy metals

After emitted, the heavy metals in FW particles can raise risks to human health. To raise the attention of public on the healthy threat of FW particles, the average amount of heavy metal exposure by inhalation (D_{inh}) per an individual's body weight over a given time span for adult and childern was calcualted by following equation (Kong et al., 2012; Yang et al., 2014):

$$D_{inh}(\mathrm{mg\,kg^{-1}\,day^{-1}}) = \frac{C \times \mathrm{InhR} \times \mathrm{EF} \times \mathrm{ED}}{\mathrm{BW} \times \mathrm{BD}} \quad (1)$$

The lifetime average daily dose (LADD) of Co, Ni, As and Cd exposure through inhalation was used for assessing cancer risk as following:

$$\mathrm{LADD} = \frac{C \times \mathrm{EF}}{\mathrm{AT} \times \mathrm{PEF}} \times \left(\frac{\mathrm{InhR_{child}} \times \mathrm{ED_{child}}}{\mathrm{BW_{child}}} + \frac{\mathrm{InhR_{adult}} \times \mathrm{ED_{adult}}}{\mathrm{BW_{adult}}}\right) \quad (2)$$

where C is exposure-point concentration. Its upper limit of the 95 % confidence interval for the mean is calculated as:

$$C_{95\,\%\,\mathrm{UCL}} = \exp\left(\overline{X} + 0.5s^2 + \frac{s \times H}{\sqrt{n-1}}\right), \quad (3)$$

ACPD
14, 28609–28655, 2014

where $\overline{X}$ is the arithmetic mean of the log-transformed data, s is the standard deviation of the log-transformed data, H is the H-statistic and n is the number of samples. InhR: inhalation rate, 7.6 and 20 $m^3\,day^{-1}$ for children and adult; EF: exposure frequency, 4 $day\,year^{-1}$ in this study (according to the discussion in Sect. 3.4.2); ED: exposure duration, 6 and 24 years for children and adult; BW: average body weight; 15 and 70 kg for children and adult; AT: the averaging time, for non-carcinogens, AT (days) = ED × 365; for carcinogens, AT (days) = 70 × 365 = 25 550.

After the D_{inh} was calculated, a Hazard Quotient (HQ) for non-cancer toxic risk can be obtained by (Kong et al., 2012):

$$HQ = D/RfD \quad (4)$$

Considering the sensitive group, the reference dose (RfD) ($mg\,kg^{-1}\,day^{-1}$) is estimated as the maximum permissible risk on human by daily exposure. The threshold values of RfD indicate whether there is adverse health effect during a life time. Then Hazard Index (HI) can be obtained by suming up the individual HQ to estimate the total risks of all elements considered:

$$HI = \sum HQ_i, \quad (5)$$

where i denotes different heavy metals. RfD values are 7×10^{-3}, 2.86×10^{-5}, 1.43×10^{-5}, 4.0×10^{-2}, 3.0×10^{-1} and 3.5×10^{-3} for the cancer risk estimation of V, Cr, Mn, Cu, Zn and Pb. For non-cancer risk estimation of Co, Ni, As and Cd, the RfD values are 5.71×10^{-6}, 2.00×10^{-2}, 3.00×10^{-4} and 1.00×10^{-3}, respectively (Kong et al., 2012). If $HI \leq 1$, there is no adverse health effects; if $HI > 1$, likely adverse health effects exist. For carcinogens, the LADD is multiplied by the corresponding RfD value. If the cancer risk is higher than 10^{-6}, risk management decisions should be made.

2.4.4 Mass closure of $PM_{2.5}$

To better understand the chemical compositions before, during and after SF, the chemical mass closure analysis was conducted. The chemical components are divided into

ACPD
14, 28609–28655, 2014

six classes as follows: mineral matter (MIN), trace elements (TE), OM, EC, sea salt (SS), secondary inorganic aerosol (SIA) and unidentified matter (UM). MIN is the sum of the common oxides of Al, Mg, Mn, Si, Na, K, Ca, Ti and Fe as:

$$\mathrm{MIN} = 2.14 \times \mathrm{Si} + 1.67 \times \mathrm{Ti} + 1.89 \times \mathrm{Al} + 1.59 \times \mathrm{Mn} + 1.67 \times \mathrm{Mg} + 1.95 \times \mathrm{Ca} + 1.35 \times \mathrm{Na} + 1.21 \times \mathrm{K} + 1.43 \times \mathrm{Fe} \quad (6)$$

As the existence of CaO and $CaCO_3$, a factor of 1.95 for Ca is used (Terzi et al., 2010). Except for the above elements in MIN, all other elements are sumed up to act as TE. OM is calculted by multiplying OC of a conversion factor, in accordance with the organic molecular carbon weight per carbon weight. Here, 2.0 is applied, same to the value used for spring festival period in Shanghai, another megacity in Yangtze Revier Delta region (Huang et al., 2012). In Allan et al. (2010), during bonfires and fireworks burning period at the Guy Fawkes' night, the OM/OC ratio ranged around 2.0 or higher than 2.0. The marine contribution is calculated based on a standard sea water composition, assuming that soluble Na^+ in aerosols only come from sea salt. Then,

$$\text{sea salt} = [\mathrm{Na^+}] + [\text{ss-}\mathrm{Cl^-}] + [\text{ss-}\mathrm{Mg^{2+}}] + [\text{ss-}\mathrm{K^-}] + [\text{ss-}\mathrm{Ca^{2+}}] + [\text{ss-}\mathrm{SO_4^{2-}}], \quad (7)$$

where $\text{ss-}\mathrm{Cl^-} = 1.8 \times [\mathrm{Na^+}]$, $\text{ss-}\mathrm{Mg^{2+}} = 0.12 \times [\mathrm{Na^+}]$, $\text{ss-}\mathrm{K^-} = 0.036 \times [\mathrm{Na^+}]$, $\text{ss-}\mathrm{Ca^{2+}} = 0.038 \times [\mathrm{Na^+}]$, and $\text{ss-}\mathrm{SO_4^{2-}} = 0.252 \times [\mathrm{Na^+}]$ (Terzi et al., 2010). SIA is the sum of nss-$\mathrm{SO_4^{2-}}$, $\mathrm{NO_3^-}$ and $\mathrm{NH_4^+}$. The concentrations of all these species in $\mu g\,m^{-3}$ are adopted.

2.4.5 Visibility re-construction by chemical components

The mass scattering efficiencies of spherical particles is a function of water and chemical components including $(NH_4)_2SO_4$, sea salt, mineral materials and carbonaceous species (Kimet al., 2001). To find which types of chemical components are the key for the visibility degration during sampling period and how can the injection of FW particles change the visibility, the IMPROVE equation was used to calculate the light extinction

ACPD
14, 28609–28655, 2014

coefficient (b_{ext}) (Kim et al., 2001; Yang et al., 2007):

$$b_{ext} = 3f(\mathrm{RH})[\text{ammonium sulfate}] + 3f(\mathrm{RH})[\text{ammonium nitrate}] + 4[\mathrm{OM}] + 1[\text{soil}] + 10[\mathrm{BC}] \quad (8)$$

The visibility can be calculated by $\mathrm{Vs} = 3.91/b_{ext}$ (Yang et al., 2007). We used [ammonium sulfate] = $0.944 \times [NH_4^+] + 1.02 \times [SO_4^{2-}]$, [ammonium nitrate] = $1.29 \times [NO_3^-]$, [OM] = 2.0 × [OC], [soil] = MIN and [BC] = [EC] (Yang et al., 2007; Tao et al., 2009). $f(\mathrm{RH})$ is the RH growth function indicating how scattering efficiencies increase for SO_4^{2-} and NO_3^- as they absorb liquid water and detailed data can be found in Tao et al. (2009).

2.4.6 WRF-FLEXPART modeling

To see the transportation distance and decreasing trend of the highest mass concentrations of $PM_{2.5}$ at CNY's Eve, Weather Research and Forecast model (WRF) version 3.4 was used to provide meteorological inputs of FLEXPART, with the NCEP global reanalysis meteorological dataset (1° × 1°) as initial and boundary conditions. The time step is set as 180 s. The grid system is divided into 28 layers in the vertical direction. Two domains are adopted, with the grid resolutions of 30 and 10 km. The simulating time period is 02:00–11:00 LT of 31 January, 2014. The output of 10 km evolution wind farms is used as the input of FLEXPART. For forward simulating of FLEXPART model, Nanjing (31°14′–32°37′ N, 118°22′–119°14′ E, height as 50 m) is considered as a whole source region. In this study, we only considered the dry and wet deposition of particles at CNY's Eve. The average mass concentration of 572 $\mu g\,m^{-3}$ is used as the initial particle concentration.

ACPD
14, 28609–28655, 2014

3 Results and discussion

3.1 Comparison of particles before, during and after Chinese Spring Festival

3.1.1 $PM_{2.5}$ mass concentrations

The concentrations of $PM_{2.5}$ (averaged as $113 \pm 69\,\mu g\,m^{-3}$, min–max: 21–318 $\mu g\,m^{-3}$) in this study by filter sampling varied consistently with those for the nine online monitoring sites set by local government at urban Nanjing (averaged as $112 \pm 70\,\mu g\,m^{-3}$, min–max: 13–385 $\mu g\,m^{-3}$) (Fig. 2b). They correlated well with correlation coefficient (R^2) higher than 0.95 ($P > 0.01$) (Supplement S6), indicating that a regional air pollution occurred in Nanjing (visibility < 10 km as Fig. 2a shown) during study period. The $PM_{2.5}$ concentrations all peaked at CNY (30 January) and LF (14 February) and the peaking values at CNY were 4–5 times of the secondary standard of China National Ambient Air Quality (75 $\mu g\,m^{-3}$, 24 h average). Results suggested that FW have obvious impacts on fine particle pollution. At CNY's Eve, two massive FW events usually occur at the evening (around 19:00–20:00 LT for the family reunion dinner) and midnight (00:00–02:00 LT for celeberating the new year). $PM_{2.5}$ showed the maximum concentrations for the two episodes as 426 ± 236 (20:00 LT) and $572 \pm 136\,\mu g\,m^{-3}$ (02:00 LT), respectively. After 02:00 LT, obviously decreasing (as exponential form, $R^2 = 0.99$) was observed. The concentrations decreased to $195 \pm 16\,\mu g\,m^{-3}$ at 13:00 LT, which was similar to that of $178 \pm 16\,\mu g\,m^{-3}$ at 17:00 LT, 30 January before extensively FW activities (Fig. 4). Note that at 30 and 31 January, the mixing layer heights were only 257 and 227 m, the wind speeds were 1.7 and 2.1 and the RH were 88 and 80 %, all favoring the accumulation of pollutants and regional air pollution formation. It was verified by the WRF-FLEXPART results which indicated that the particles with highest mass concentrations at 02:00 LT moved outside of Nanjing in the following nine hours. The center with peaked particle mass concentrations transported about 285 km to the north of Naning (Supplement S7) and the decreasing trend was in accordance with the real particle concentrations decreasing (Fig. 5). The injection of FW particles deteri-

ACPD
14, 28609–28655, 2014

orated the air quality, with visibilities descreased to 1.4–6.2 km in the following three days. Therefore, the $PM_{2.5}$ pollution raised by FW can last for at least three days under unfavorable weather conditions (visibility was strongly related to $PM_{2.5}$ mass in 30 January–3 February, R^2 = 0.82). At 3 and 5 February, $PM_{2.5}$ was cleaned effectively by the rainfall (precipitation as 0.3 and 9 mm), descreasing by 5.6–10.6 times for the ten sites.

3.1.2 Characteristic of chemical species

Tables 1 and 2 summarized the statistics of $PM_{2.5}$, water-soluble ions, OC and EC before, during and after SF. The data at CNY and LF were listed separately for intensive FW avtivities. The ratios of $PM_{2.5}$ and chemical species at CNY and LF with those for the day before them were also listed. For elements, K, Si, Al, Na, Ca and Fe were the most abundant species, totally accounting for 85–90 % for all of the elements at these five periods. Without considering the data for CNY, elements Al, K, Ba and Sr at SF still elevated when compared with those for Pre-SF, whereas all other elements descrased during SF. This was related to the weakened sources, like construction activities, vehicle emission and industrial activities in the national holiday. For ions, NO_3^- was most abundant, averaged as 5.9 (±3.7) $\mu g\,m^{-3}$ for the days without intensive FW activities, then followed by SO_4^{2-} and NH_4^+, with average concentrations of 5.0 (±3.7) and 4.8 (±2.4) $\mu g\,m^{-3}$, respectively. K^+ and Cl^- also had relatively high concentrations of 0.9 (±1.0) and 0.8 (±0.5) $\mu g\,m^{-3}$. It was similar to the results of Wang et al. (2014) that the secondary aerosols in Nanjing are dominated by nitrate in winter haze periods. Na^+, Ca^{2+}, Mg^{2+}, F^- and NO_2^- accounted for a minor fraction (totally of 4.2 %). For carbonaceous species, OC3, OC4 and EC1 were most abundant, in combination accouting for 80 % of the total carbon, indicating coal combusition and gasoline exhaust were important sources for $PM_{2.5}$ at Nanjing (Cao et al., 2005). OPC and OC1 also showed a higher values which may be related to biomass burning (Cao et al., 2005). NO_3^-, OC and EC were highest for Pre-SF period, as the "spring travel rush" effect, characterized by extremely high traffic flows (Huang et al., 2012). The $PM_{2.5}$ concentrations

ACPD
14, 28609–28655, 2014

descreased for about 10 $\mu g\,m^{-3}$ during SF, implying that the reduction of anthropologic sources in this national holiday (Feng et al., 2012). The particle concentration lower than that for pre-holiday period was also found in Shanghai (Huang et al., 2012).

During CNY with intensive FW, concentrations of Ba and Sr exhibited the most significant increase, by factors of 99.1 and 79.4 compared to the day before CNY (Pre-CNY). Ba and Sr also showed the highest ratios for LF/Pre-LF (the day before LF), as 9.7 and 5.7, respectively. Then followed by EC2, OC1, K, K^+, Al, Bi, SO_4^{2-}, OC2, EC1 and OC, going up to 33.7–4.1 times for CNY/Pre-CNY, respectively. Other species increased by 1.2–3.8 times except for W (0.6), Na^+ (0.7), NO_2^- (0.8) and OC4 (0.9). It implied that Na^+ was not affected by the FW and can be used as the tracer of sea salt. Most species also increased at LF when compared with Pre-LF, but the increasing ratios were much lower than those at CNY. It can be explained as the FW at LF (there are only organized FW activities by some organizations at cities) were less intensive than that at CNY (FW activities are national spread, from city to small villages). Crustal elements like Li, Be, Si, Na, Ca, Ti and Mn increased by about 1–2 times during FW, indicating the use of clay in firework production. Ca^{2+} and EC1 decreased by factors of 0.8 and 0.9, suggesting the increase of construction activities and vehicle emissions after SF. Meanwhile, Ba and Sr tend to be tracers of firework (R^2 = 0.99), consistent with former studies (Estrellan and Iino, 2010; Sarkar et al., 2010; Feng et al., 2012). As shown in the Supplement S2 and literature (Moreno et al., 2007; Vecchi et al., 2008; Joly et al., 2010; Sarkar et al., 2010; Richard et al., 2011; Do et al., 2012; Tsai et al., 2012; Jing et al., 2014), the compounds of these elments are important FW manufacturing materials. Barium compounds can be used as oxidiser ($BaClO_3$ and $Ba(NO_3)_2$). $Sr(NO_3)_2$ can be used to give red color fireworks and potassium compounds are the most important compositions of black powder (as KNO_3 or $KClO_3$). Al is used alone as a common constituent for fuel, or to form sparks and glitter effects or as alloy magnalium (50 : 50 Mg : Al) for sparks and crackling stars. Fireworks also contain charcoal (Joly et al., 2010; Sarkar et al., 2010; Tsai et al., 2012) and organic materials are used as adhesive, such as polyvinyl alcohol, polyoxyethylene, phenol formaldehyde resin

ACPD
14, 28609–28655, 2014

and shell-lac. They are responsible for the evelated concentrations of EC2 (Joly et al., 2010; Sarkar et al., 2010; Tsai et al., 2012) and OC1 during FW periods.

3.2 Mass closure and re-construction of visibility

Figure 6 illustrates the $PM_{2.5}$ mass balance of MIN, TE, OM, EC, SS, SIA and UM. About 60 % of the chemical species in $PM_{2.5}$ were detected. The unaccounted PM mass were explained by the following four reasons: (1) non-C atoms in organic aerosols; (2) sampling and measurement artefacts; (3) conversion factors used for OM and MIN calculating; (4) aerosol water content (Tsyro, 2005; Terzi et al., 2010). Water constituted 20–35 % of the annual mean PM_{10} and $PM_{2.5}$ concentrations (Tsyro, 2005). At 6 February, the water content in $PM_{2.5}$ was high to 72 %, indicating the influence of rainfall and high RH (90 %). These also lead to the gravimetrically measured particulate mass (PM_{meas}) higher than the mass calculated by adding individual components (PM_{meas}), while tight correlations still existed between them (PM_{meas} = $1.52PM_{cal} + 14.5$, $R^2 = 0.91$). The slope was similar to those as 1.02–1.42 in Terzi et al. (2010).

The averaged chemical components of $PM_{2.5}$ profiles exhibited OM (26 %) > SIA (18 %) > MIN (9 %) > EC (3.9 %) > SS (1.7 %) > TE (0.67 %). The OM, TE and EC descreased in SF (as 23, 0.6 and 2.7 %) when compared with those at Pre-SF (as 34, 0.7 and 6.2 %). These changes reflected the holidy effect i.e. at the SF holidy, the new injection of FW particles cannot offset the reduced particles from vechicle emission and/or to industrial sources, especially for organic matter, trace elements and elemental carbon, which are important compositions of vehicle exhausts and industrial avtivities. At CNY, obviously elevated OM was observed, accounting for 39.3 % of $PM_{2.5}$. While SIA was only 14.4 %, with the peak values occurred at 3 February (as 36 %), suggesting that after intensive emission of FW pollutants at CNY's Eve, secondary ions were gradually formed during aging processes through gas-particles transformation of SO_2 and NO_x, etc. It should be emphasized that MIN and TE were both important compositions of $PM_{2.5}$, totally accounting for 5.8–18.5 %. In a recent study by AMS for aerosols dur-

ACPD
14, 28609–28655, 2014

ing Chinese Spring Festival at Beijing, organics, nitrate, sulfate, ammonium, BC and chloride, accounted for 43, 22, 14, 13, 5 and 3 % of $PM_{1.0}$ with no elements considered (Jiang et al., 2014). The combination of filter sampling-offline chemical analysis and online real-time monitoring of chemcial species are desired for atmospheric aerosol studies.

Figure 7a shows the calculated average values of extinction coefficient (b_{ext}). They varied between 44 and 525 $M m^{-1}$. The calculated visibility (V_{cal}) exhibited good correlations with the measured one (V_{meas}) ($V_{cal} = 0.96V_{meas} + 1.4$, $R^2 = 0.45$, $P < 0.001$). The discrepancy between the measured and calculated values can be attributed to the influence of ambient water vapor (Huang et al., 2012) which was a key component of aerosol particles in this study as discussed before. At higher RH, the role of ambient water vapor on light extinction was more important (Huang et al., 2012). The b_{ext} exhibited higher values at CNY and the following three days, in the range of 301–525 $M m^{-1}$. $(NH_4)_2SO_4$ had the largest contribution to b_{ext}, accounting for 36.5 ± 11.7 %, followed by NH_4NO_3 (25.8 ± 8.2 %), EC (21.8 ± 9.0 %), OM (10.8 ± 4.2 %) and soil (5.1 ± 1.8 %) (Fig. 7b). These results implied that sulfate was the largest contributor to visibility degradation especially at SF period. Before SF, the contribution of EC can be as high as 34–44 % during serious haze periods (24–26 January, RH < 51 %). It highlights the importance of controlling vehicle emissions in haze days. Sulfate and soot were also found as the main contributors to visibility degradation in other studies (Tao et al., 2009). The results obtained here were different from those in Shanghai that organic aerosol had the largest contribution to the aerosol extinction as 47 %, then followed by sulfate ammonium (22 %), nitrate ammonium (14 %) and EC (12 %) (Huang et al., 2012). The FW at CNY obviously changed the contributions of chemical species to scattering coefficient. At CNY, the influence of FW particles to visibility was mainly controlled by $(NH_4)_2SO_4$ (36 %), NH_4NO_3 (26 %), EC (15 %) and OM (15 %). During FW particle aging processes, the contribution of $(NH_4)_2SO_4$ increased from 36 % (30 January) to 67 % (3 February), while for NH_4NO_3, its contribution increased first to 28 % at 31 January and then decreased to 10 % (3 February). Similar trend was found for EC,

ACPD
14, 28609–28655, 2014

it increased to 22 % (1 February) and then decreased to 7.6 % (3 February). For OM, it exhibited decreasing trend, to the lowest value at 2 February (5.5 %).

3.3 Source evolution

3.3.1 Contributions of fireworks burning to $PM_{2.5}$ at CNY and LF

The $PM_{2.5}$ concentrations peaked at CNY and LF in this study with intensive FW activities. Assuming that the $PM_{2.5}$ collected on CNY and LF was a simple combination of particles from FW and other emission sources, the contribution and compositions of the particles from FW can be estimated by substracting the contribution of the non-firework sources (Feng et al., 2012). An accumulation factor of 0.88 (mixing layer heights at 30 and 29 January were 227 and 257 m, respectively) and 0.51 (mixing layer heights at 14 and 13 February were 353 and 696 m, respectively) were used to eliminate the disperse impact caused by mixing height layer increasing (Feng et al., 2012; Deka and Hoque, 2014). About 60.1 and 10.9 % of the $PM_{2.5}$ masses at CNY and LF were estimated to be from FW. The contributions to almost all species of FW at CNY were more obvious than those at LF (Fig. 8). At CNY, OPC, EC3, Ba, Sr, Soot-EC, EC2 and OC1 maintained the higher contributions from FW, larger than 80 %, followed by K, K^+, Al, Bi and Char-EC, with the contributions higher than 70 %. At LF, 45 % of Ba and 41 % of Sr were from FW and the contributions to V, Bi, Fe, Be, K, K^+, Al, NO_2^- and Sb were higher than 20 %.

3.3.2 Source variations by tracers and PCA analysis

In order to further identify the sources of particles, PCA results are shown in Fig. 9 and Supplement S8.

Five, five and eight factors were extracted for the dataset of Pre-SF, SF and After-SF period, which explained 100, 99.4 and 97.5 % of the variance, suggesting almost all the sources have been explained. Fireworks burning was the most important source for

ACPD
14, 28609–28655, 2014

$PM_{2.5}$, contributing 24.0 % for the whole period. Coal combustion (including both local and regional transport) was also important to $PM_{2.5}$ at this site in winter (contributing 19.3 %). It was verified by the time series of tracers (As and Sb, highly correlated with R^2 = 0.88) for coal combustion in Fig. 10a. Extremly high values can be found at 24 January, even higher than those for the intensive FW day. This can be explained by two reasons: (1) on 24 January, it was a haze day with visibility and mixing layer height as 8.2 km and 321 m, facilitating the acculumation of pollutants; (2) the air masses on 24 January were classified as cluster 2 from central China where the Chang-Zhu-Tan region with intensive non-ferrous metal metallurgy industries with huge coal consumption is located. On this day, higher concentrations were also found for metals like Mg (228 ng m^{-3}), Cr (17 ng m^{-3}), Ca (782 ng m^{-3}), Mn (85 ng m^{-3}), Fe (1014 ng m^{-3}), Co (0.61 ng m^{-3}), Ni (7.6 ng m^{-3}), Cu (124 ng m^{-3}), Mo (4.4 ng m^{-3}), Cd (8.8 ng m^{-3}), Sn (16 ng m^{-3}) and Pb (359 ng m^{-3}). FW contributed about half of the $PM_{2.5}$ during SF. For Pre-SF and After-SF periods, its contributions were 9 and 14 %. As shown in Fig. 10b, the tracers of Ba and Sr exhibited much higher values at SF, and there were also some small peaks before SF (27 January) and after SF (14 February). During the one-week holiday, most industrial activities shut down in China with low energy consumption during this period (Feng et al., 2012; Huang et al., 2012; Li et al., 2013). As holiday effect, when compared the source contributions at SF to those at Pre-SF, the contributions of coal combustion descreased from 46 to only 16 %, the contributions of vehicle emissions decreased from 17 to 14 % and the contributions of dust also descreased significantly. For After-SF period, along with the gradually re-starting of industrial plants and contrustion activities and increasing traffic density, the contributions from coal combustion, heavy oil burning, industrial processes and road dust increased, to 37, 4, 3.4 and 5 %, respectively. OC and EC wers selected as the tracers of vehicle emission and their correlation was higher to 0.80 without the data at CNY and LF. Ca was selected as the tracer for construction activities or road dust (the main road was covered by abundant dust from subway construstion). Na^+ was used as the tracer of sea salt. Li, Be and Si were selected as the indicators of soil (R^2 higher than 0.65 between them). The vari-

ACPD
14, 28609–28655, 2014

ations of mass concentrations of these tracers before, during and after SF coincided with the contributions of corresponding sources.

3.4 Aging processes

3.4.1 The aging processes and mechanisms of fireworks burning particles

Previous studies indicated that the aerosol emission from FW activities is a short-term air quality degradation event (Jing et al., 2014), but no studies concerned how long the duration time is, and during the aging processes, what are the substantial hazard risk levels raised by elevated heavy metals from intensive FW. To better understand the influence of FW particles, its aging processes after emission were analyzed. It should be emphasized that at SF, contributions from other human sources were low (Fig. 9), so the air quality in these days was mainly influenced by the highest contributor-FW particles' aging processes, including deposition, dispersion and transformations.

From Figs. 2b and 10b, it can be seen that it takes abut four days for the highest $PM_{2.5}$ and FW tracers-Ba and Sr at CNY to step down to the normal values of pre-CNY. The same situations were found for K^+, Cl^-, NH_4^+ and NO_3^- (Fig. 11a). But for SO_4^{2-}, six days (until 5 February) were needed to reduce its concentration to the level of 29 January. On 1 February, though $PM_{2.5}$ has descreased from 317 to 185 $\mu g\,m^{-3}$, the visibility was still low as 2.2 km, with peak concentrations of NH_4^+, NO_3^- and SO_4^{2-} (they contributed 65 % of the b_{ext}). On 3 February, $PM_{2.5}$ descreased to 30 $\mu g\,m^{-3}$, haze pollution still existed with the visibility as 6.7 km, mainly contributed by ammonium sulfate (67 %). Until 5 February, after one day of rainfall, SO_4^{2-} decreased to 2.0 $\mu g\,m^{-3}$, lower than that on 29 January (3.7 $\mu g\,m^{-3}$). While ammonium sulfate was still the highest contributor to b_{ext} (49 %). As there was a break after 6 February, it can be concluded that the intensive FW particles at CNY's Eve can influence the air quality for at least 6 days by changing the main contributors of extinction coefficient as EC + OM to ammonium sulfate even though there was a rainfall (9 mm).

ACPD
14, 28609–28655, 2014

Pollution gases (SO_2, NO_x, etc.) emitted during FW events may be oxidized to secondary organic and inorganic components that may be adsorbed onto particles (Sarkar et al., 2010). From Fig. 11a, we can find that Ca^{2+}, NH_4^+, NO_3^- and SO_4^{2-} showed peak values at CNY and two days after, suggesting the directly emission from FW and secondary formations through heterogeneous reactions of SO_2 and NO_x on crustal materials. Higher correlations were found for NO_3^--Ca^{2+} ($R^2 = 0.64$) and SO_4^{2-}-Ca^{2+} ($R^2 = 0.70$). The lower wind speed (1.7–2.6 m s^{-1}) and mixing layer heights (257–284 m) helped to capture pollution gases near the ground and higher RH (74–88 %) favored their secondary transformation and following condensation onto pre-existing aerosols at the initial four days after intesive FW on CNY.

From 30 January to 4 February, the ratios of soot-EC/NO_3^-, Cl^-/K^+, NO_3^-/SO_4^{2-} and Ca^{2+} decreased first and then increased again, while to the opposite for SO_4^{2-}/K^+, suggesting the secondary formation (Fig. 11b). Secondary formations of NH_4^+, NO_3^- and SO_4^{2-} from the gases emitted from FW were also found in other cities (Wang et al., 2007; Yang et al., 2014). During aging, the direct emission of KCl from fireworks ($R^2 = 0.85$ for K^+-Cl^-) can react with H_2SO_4 and HNO_3 to form SO_4^{2-} ($R^2 = 0.76$ for K^+-SO_4^{2-}) and NO_3^- ($R^2 = 0.96$ for K^+-NO_3^-), leading to the desreasing of Cl^-/K^+ ratio and increasing of SO_4^{2-}/K^+ ratio. Li et al. (2013) drew the same conclusion through single particle analysis method as that K-rich particles containing significant amounts of S in the form of K_2SO_4 at a background site under the influence of FW. It implied the existence of the aging of fresh FW particles via heterogeneous reactions during long-range transport. Soot (soot-EC) can be directly introduced by firework displays (Do et al., 2012) which showed moderate correlations with NO_3^- and SO_4^{2-} ($R^2 = 0.47$ and 0.56, respectively) in this study, indicating the coating of NO_3^- and SO_4^{2-} on soot. The OC/EC ratio peaked on CNY (as 6.8) which was mainly contributed by the increasing of OC1, OC2 and OPC. They are related with volatilization of the organic materials used for fireworks producing. The smelting point temperatures for polyvinyl alcohol, polyoxyethylene and shell-lac are 230–240, 212, 115–120 °C and the softening point

ACPD
14, 28609–28655, 2014

for phenol formaldehyde resin is 80–85 °C, all lower than the measuring temperature for OC2 (230 °C). Therefore, OC1, OC2 and OPC are more easily and directly emitted from FW. The iniatially decreasing OC/EC ratio indicated the gradual formation of secondary (aged) organic aerosols (Feng et al., 2012). To summarize, the heterogeneous reactions of SO_2 and NO_x on crustal materials directly from FW, the replacement of Cl^- by NO_3^- and SO_4^{2-}, coating of NO_3^- and SO_4^{2-} on soot and formation of secondary organic aerosols are the main of FW particles' aging mechanisms.

Previous studies also incidated that metals like Fe, Cu and Mn can catalyze the formation of NO_3^- and SO_4^{2-} (Wang et al., 2007; Do et al., 2012; Feng et al., 2012). Wang et al. (2007) indicated that the heterogeneous formation of sulfate through reacting with a-Fe_2O_3 exsits under moist atmosphere and is a function of RH and HNO_3. As shown in Fig. 12 and Supplement S9, sigificant correlations are found between NO_3^- and Fe, Cu and Mn and between SO_4^{2-} and Fe, Cu and Mn at higher RH. It indicated the mechanism of metal-catalyzed formation of NO_3^- and SO_4^{2-} was more likely to occur at higher RH. At the day of CNY and 2 February, the RH was 88 and 87 %, implying the occurrence of metal-catalyzed reactions, which may also explain the higher NO_3^- and SO_4^{2-} concentrations at these days. The R^2 increased with the elevated RH. There are significant increases of R^2 for Fe-NO_3^-, Mn-NO_3^- and Cu-NO_3^- when RH were > 85 %, > 85 % and > 65 %, respectively. For the correlations of Fe-SO_4^{2-}, Mn-SO_4^{2-} and Cu-SO_4^{2-}, clear increasings in R^2 were found when RH were > 85 %, > 85 % and > 55 %. Then we can conclude that for Fe-catalyzed and Mn-catalyzed reactions, the threhold of RH was around 85 %; for Cu-catalyzed formation of NO_3^- and SO_4^{2-}, the threholds of RH were around 65 and 55 %, respectively. For RH higher than 90 %, the R^2 decreased for Fe-NO_3^-, Cu-NO_3^-, Fe-SO_4^{2-} and Mn-SO_4^{2-} which needs more data in the future to be verified and explained.

ACPD
14, 28609–28655, 2014

3.4.2 Potential health risks during the aging of fireworks burning particles

After emitted from the intensive FW at CNY's Eve, heavy metals including Vi, Cr, Mn, Co, Ni, Cu, Zn, As, Cd and Pb decreased directly in the following four days (Supplement S10). It indicated that they were emitted from FW primarily and were removed mainly by dispersion and deposition during aging. Then we can assume that: (1) other emisson sources (coal combustion, vehicle exhaust and industrial processes were their main sources) for these metals were stable during SF period; (2) the highest concentrations of them were just the combinations of particles from the FW on 30 January and other sources on 29 January. We subtract the concentrations of elements at 29 January from the corresponding values on 30 and 31 January, 1 and 2 February for each element, respectively, to obtain the elements concentrations just related with the FW particles. Considering the variations of mixing layer height (as 306, 257, 227, 284 and 248 m for the five days of 29 January–2 February) and accumulation effect, the concentrations of these elements on 30 and 31 January, 1 and 2 February were transferred by factors of 0.84, 0.74, 0.93 and 0.81, respectively. Then the $C_{95\,\%\,\mathrm{UCL}}$ values raised by FW particles were 7.4, 21.2, 12.0, 23.7, 0.42, 5.2, 54.5, 11.7, 126 and 837 ng m^{-3} of the ten elements, respectively, for the four days. The non-cancer risks raised just by FW at CNY's Eve were below 1 (0.03 and 0.02 for childern and adult) (Fig. 13), indicating no adverse health effects. However the cancer risk was 1.62×10^{-6}, higher than 10^{-6}, suggesting the FW particles were important carcinogens and should be controlled effectively especially for the contained Cd and As. Meanwhile, the risk level for childern was higher than that for adult, which meant that children were more sensitive to non-carcinogenic effects and should be kept from possible exposure to them (Yang et al., 2014). Therefore, the FW should be restricted at SF from the view of their cancer risks to human health.

ACPD
14, 28609–28655, 2014

4 Conclusions

Thirty-nine elements, ten water-soluble ions and eight fractions of carbonaceous species were measured to fully characterize the chemcial compositions in atmospheric $PM_{2.5}$ in Nanjing during the 2014 Chinese Spring Festival (SF). Serious regional haze pollution occurred and lasted during the whole sampling period. At the Chinese New Year (CNY)'s Eve, after it peaked at 02:00 LT, $PM_{2.5}$ exponentially decreased in the following 11 h to the level before extensive fireworks burning (FW) activities. Due to holiday effect, almost all elments decreased during SF except for Al, K, Ba and Sr which were related with FW. As the "spring travel rush" effect, NO_3^-, OC and EC showed highest values for periods before SF, indicating the extremely high traffic flows. At the New Year's Eve, about 60.1 % of the $PM_{2.5}$ mass was estimated to be from FW. Highly elevated Ba and Sr were also found and highly correlated, indicating they can be used as the tracers of FW. The intensive FW at CNY's Eve obviously changed the chemical compositions of $PM_{2.5}$, with elevated organic matter (OM) immediately, contributing 39.3 % of $PM_{2.5}$. The contributions of secondary ions formed by gas-particle transformations gradually increased during FW particles'aging processes. After FW particles emitted at CNY, the contribution of $(NH_4)_2SO_4$ to extinction coefficient increased from 36 to 67 %; while for NH_4NO_3 and EC, their contributions increased first and then decreased. According to tracers and principle component analysis, fireworks burning was the most important source of $PM_{2.5}$ at this site. FW contributed about half of $PM_{2.5}$ during SF. Tracers for various sources (As and Sb for coal combustion, Ba and Sr for FW, OC and EC for vehicle emission, Ca for construction or road dust, Na^+ for sea salt and Li, Be and Si for soil) perfomed well and they varied accordantly with the contributions of corresponding sources. The FW particles emtted from CNY's Eve may undergo at least six days aging processes from the decreasing trend of SO_4^{2-}. The aging processes were characterized by heterogeneous reactions of SO_2 and NO_x on crustal materials directly from FW, the replacement of Cl^- by NO_3^- and SO_4^{2-}, coating of NO_3^- and SO_4^{2-} on soot, formation of secondary organic aerosols and metal-catalyzed formation

ACPD
14, 28609–28655, 2014

of NO_3^- and SO_4^{2-} at higher relative humidity. For Fe-catalyzed and Mn-catalyzed reactions, the threholds of RH were around 85 %; while for Cu-catalyzed formations of of NO_3^- and SO_4^{2-}, the threholds of RH were around 65 and 55 %, respectively. During the aging processes, FW particles at CNY obviously changed the main contributors to the visibility from EC + OM to ammonium sulfate. Meanwhile, higher cancer risks raised by heavy metals (especially for Cd and As) only related with FW particles emitted at CNY's Eve was 1.62×10^{-6}, which impose higher non-cancer risks to childern than adult. The results in this study will be useful for understanding the detailed compositions and aging processes of FW particles and also highlight the importance of controlling intensive fireworks burning in order to protect air quality and reduce the cancer risks.

The Supplement related to this article is available online at doi:10.5194/acpd-14-28609-2014-supplement.

Acknowledgements. This work was funded by the National Natural Sciences Foundation of China (No. 41030962), Scientific and technological cooperation between the Government of China-Serbia (2013(158)2-10), the grant of China Scholarship Council and the Priority Academic Program Development (PAPD) of Jiangsu Higher Education Institution.

References

Allan, J. D., Williams, P. I., Morgan, W. T., Martin, C. L., Flynn, M. J., Lee, J., Nemitz, E., Phillips, G. J., Gallagher, M. W., and Coe, H.: Contributions from transport, solid fuel burning and cooking to primary organic aerosols in two UK cities, Atmos. Chem. Phys., 10, 647–668, doi:10.5194/acp-10-647-2010, 2010.

Attri, A. K., Kumar, U., and Jain, V. K.: Microclimate: formation of ozone by fireworks, Nature, 411, 1015, 2001.

Cao, J. J., Wu, F., Chow, J. C., Lee, S. C., Li, Y., Chen, S. W., An, Z. S., Fung, K. K., Watson, J. G., Zhu, C. S., and Liu, S. X.: Characterization and source apportionment of atmo-

ACPD
14, 28609–28655, 2014

spheric organic and elemental carbon during fall and winter of 2003 in Xi'an, China, Atmos. Chem. Phys., 5, 3127–3137, doi:10.5194/acp-5-3127-2005, 2005.
Deka, P. and Hoque, R. R.: Incremental effect of festive biomass burning on wintertime PM_{10} in Brahmaputra Valley of Northeast India, Atmos. Res., 143, 380–391, 2014.
Do, T. M., Wang, C. F., Hsieh, Y. K., and Hsieh, H. F.: Metals present in ambient air before and after a firework festival in Yanshui, Tainan, Taiwan, Aerosol Air Qual. Res., 12, 981–993, 2012.
Dutschke, A., Lohrer, C., Kurth, L., Seeger, S., Barthel, M., and Panne, U.: Aerosol emissions from outdoor firework displays, Chem. Eng. Technol., 12, 2044–2050, 2011.
Estrellan, C. R. and Iino, F.: Toxic emissions from open burning, Chemosphere, 80, 193–207, 2010.
Feng, J. L., Sun, P., Hu, X. L., Zhao, W., Wu, M. H., and Fu, J. M.: The chemical composition and sources of $PM_{2.5}$ during the 2009 Chinese New Year's holiday in Shanghai, Atmos. Res., 118, 435–444, 2012.
Godri, K. J., Green, D. C., Fuller, G. W., OSTO, M. D., Beddows, D. C., Kelly, F. J., Harrison, R. M., and Mudway, I. S.: Particulate oxidative burden associated with firework activity, Environ. Sci. Technol., 44, 8295–8301, 2010.
Han, Y. M., Han, Z. W., Cao, J. J., Chow, J. C., Watson, J. G., An, Z. S., Liu, S. X., and Zhang, R. J.: Distribution and origin of carbonaceous aerosol over a rural high-mountain lake area, Northern China and its transport significance, Atmos. Environ., 42, 2405–2414, 2008.
Han, Y. M., Cao, J. J., Lee, S. C., Ho, K. F., and An, Z. S.: Different characteristics of char and soot in the atmosphere and their ratio as an indicator for source identification in Xi'an, China, Atmos. Chem. Phys., 10, 595–607, doi:10.5194/acp-10-595-2010, 2010.
Huang, K., Zhuang, G., Lin, Y., Wang, Q., Fu, J. S., Zhang, R., Li, J., Deng, C., and Fu, Q.: Impact of anthropogenic emission on air quality over a megacity – revealed from an intensive atmospheric campaign during the Chinese Spring Festival, Atmos. Chem. Phys., 12, 11631–11645, doi:10.5194/acp-12-11631-2012, 2012.
Jiang, Q., Sun, Y. L., Wang, Z., and Yin, Y.: Aerosol composition and sources during the Chinese Spring Festival: fireworks, secondary aerosol, and holiday effects, Atmos. Chem. Phys. Discuss., 14, 20617–20646, doi:10.5194/acpd-14-20617-2014, 2014.

ACPD
14, 28609–28655, 2014

Jing, H., Li, Y. F., Zhao, J. T., Li, B., Sun, J. L., Chen, R. Gao, Y. X., and Chen, C. Y.: Wide-range particle characterization and elemental concentration in Beijing aerosol during the 2013 Spring Festival, Environ. Pollut., 192, 204–211, 2014.

Joly, A., Smargiassi, A., Kosatsky, T., Fournier, M., Dabek-Zlotorzynska, E., Celo, V., Mathieu, D., Servranckx, R., D'amours, R., Malo, A., and Brook, J.: Characterisation of particulate exposure during fireworks displays, Atmos. Environ., 44, 4325–4329, 2010.

Kang, H. Q., Zhu, B., Su, J. F., Wang, H. L., Zhang, Q. C., and Wang, F.: Analysis of a long-lasting haze episode in Nanjing, China, Atmos. Res., 120–121, 78–87, 2013.

Kim, K. W., Kim, Y. J., and Oh, S. J.: Visibility impairment duringYellow Sand periods in the urban atmosphere of Kwangju, Korea, Atmos. Environ., 35, 5157–5167, 2001.

Kong, S. F., Han, B., Bai, Z. P., Chen, L., Shi, J. W., and Xu, Z.: Receptor modeling of $PM_{2.5}$, PM_{10} and TSP in different seasons and long-range transport analysis at a coastal site of Tianjin, China, Sci. Total Environ., 408, 4681–4694, 2010.

Kong, S. F., Lu, B., Ji, Y. Q., Zhao, X. Y., Bai, Z. P., Xu, Y. H., Liu, Y., and Jiang, H.: Risk assessment of heavy metals in road and soil dust within $PM_{2.5}$, PM_{10} and PM_{100} fractions in Dongying city, Shandong Province, China, J. Environ. Monitor., 14, 791–803, 2012.

Kong, S. F., Ji, Y. Q., Lu, B., Zhao, X. Y., Chen, L., Bai, Z. P., Xu, Y. H., Liu, Y., and Jiang, H.: Characteristic of $PM_{2.5}$, PM_{10} and TSP source profiles for fugitive dust in a coastal oilfield city, China, Aerosol Air Qual. Res., accepted, doi:10.4209/aaqr.2013.06.0226, 2014a.

Kong, S. F., Wen, B., Chen, K., Yin, Y., Li, Q., Li, L., Yuan, L., and Sun, X.: Ion chemistry for atmospheric size-segregated aerosol and depositions at an offshore site of Yangtze River Delta (YRD) region, China, Atmos. Res., 147–148, 205–226, 2014b.

Li, L., Yin, Y., Kong, S. F., Wen, B., Chen, K., Yuan, L., and Li, Q.: Altitudinal effect to the size distribution of water soluble inorganic ions in PM at Huangshan, China, Atmos. Environ., 98, 242–252, 2014.

Li, M. N. and Zhang, L.: Haze in China: current and future challenges, Environ. Pollut., 189, 85–86, 2014.

Li, P. H., Han, B., Huo, J., Lu, B., Ding, X., Chen, L., Kong, S. F., Bai, Z. P., and Wang, B.: Characterization, meteorological influences and source identification of carbonaceous aerosol during autumn-winter period in Tianjin, China, Aerosol Air Qual. Res., 2, 283–294, 2012.

Li, W. J., Shi, Z. B., Yan, C., Yang, L. X., Dong, C., and Wang, W. X.: Individual metal-bearing particles in a regional haze caused by firecracker and firework emissions, Sci. Total Environ., 443, 464–469, 2013.

ACPD
14, 28609–28655, 2014

Moreno, T., Querol, X., Alastuey, A., Minguillón, M. C., Pey, J., Rodriguez, S., Miró, J. V., Felis, C., and Gibbons, W.: Recreational atmospheric pollution episodes: inhalable metalliferous particles from firework displays, Atmos. Environ., 41, 913–922, 2007.

Richard, A., Gianini, M. F. D., Mohr, C., Furger, M., Bukowiecki, N., Minguillón, M. C., Lienemann, P., Flechsig, U., Appel, K., DeCarlo, P. F., Heringa, M. F., Chirico, R., Baltensperger, U., and Prévôt, A. S. H.: Source apportionment of size and time resolved trace elements and organic aerosols from an urban courtyard site in Switzerland, Atmos. Chem. Phys., 11, 8945–8963, doi:10.5194/acp-11-8945-2011, 2011.

Sarkar, S., Khillare, P. S., Jyethi, D. S., Hasan, A., and Parween, M.: Chemical speciation of respirable suspended particulate matter during a major firework festival in India, J. Hazard. Mater., 184, 321–330, 2010.

Shen, Z. X., Cao, J. J., Arimoto, R., Han, Z. W., Zhang, R. J., Han, Y. M., Liu, S. X., Okuda, T., Nakao, S., and Tanaka, S.: Ionic omposition of TSP and $PM_{2.5}$ during dust storms and air pollution episodes at Xi'an, China, Atmos. Environ., 43, 2911–2918, 2009.

Tan, P. H., Chou, C., Liang, J. Y., Chou, C. C. K., and Shiu, C. J.: Air pollution "holiday effect" resulting from the Chinese New Year, Atmos. Environ., 43, 2114–2124, 2009.

Tao, J., Ho, K. F., Chen, L. G., Zhu, L. H., Han, J. L., and Xu, Z. C.: Effect of chemical composition of $PM_{2.5}$ on visibility in Guangzhou, China, 2007 spring, Particuology, 7, 68–75, 2009.

Terzi, E., Argyropoulos, G., Bougatioti, A., Mihalopoulos, N., Nikolaou, K., and Samara, C.: Chemical composition and mass closure of ambient PM_{10} at urban sites, Atmos. Environ., 44, 2231–2239, 2010.

Tian, Y. Z., Wang, J., Peng, X., Shi, G. L., and Feng, Y. C.: Estimation of the direct and indirect impacts of fireworks on the physicochemical characteristics of atmospheric PM_{10} and $PM_{2.5}$, Atmos. Chem. Phys., 14, 9469–9479, doi:10.5194/acp-14-9469-2014, 2014.

Tsai, H. H., Chien, L. H., Yuan, C. S., Lin, Y. C., Jen, Y. H., and Ie, I. R.: Influences of fireworks on chemical characteristics of atmospheric fine and coarse particles during Taiwan's Lantern Festival, Atmos. Environ., 62, 256–264, 2012.

Tsyro, S. G.: To what extent can aerosol water explain the discrepancy between model calculated and gravimetric PM_{10} and $PM_{2.5}$?, Atmos. Chem. Phys., 5, 515–532, doi:10.5194/acp-5-515-2005, 2005.

Vecchi, R., Bernardoni, V., Cricchio, D., Alessandro, A. D., Fermo, P., Lucarelli, F., Nava, S., Piazzalunga, A., and Valli, G.: The impact of fireworks on airborne particles, Atmos. Environ., 42, 1121–1132, 2008.

ACPD
14, 28609–28655, 2014

Wang, H. L., An, J. L., Shen, L. J., Zhu, B., Pan, C., Liu, Z. R., Liu, X. H., Duan, Q., Liu, X., and Wang, Y. S.: Mechanism for the formation and microphysical characteristics of submicron aerosol during heavy haze pollution episode in the Yangtze River Delta, China, Sci. Total Environ., 490, 501–508, 2014.

Wang, Q. Y., Cao, J. J., Shen, Z. X., Tao, J., Xiao, S., Luo, L., He, Q. Y., and Tang, X. Y.: Chemical characteristics of $PM_{2.5}$ during dust storms and air pollution events in Chengdu, China, Particuology, 11, 70–77, 2013.

Wang, Y., Zhuang, G. S., Xu, C., and An, Z. S.: The air pollution caused by the burning of fireworks during the lantern festival in Beijing, Atmos. Environ., 41, 417–431, 2007.

Wehner, B., Wiedensohler, A., and Heintzenberg, J.: Submicrometer aerosol size distribution and mass concentration of the millennium fireworks 2000 in Leipzig, Germany, J. Aerosol Sci., 12, 1489–1493, 2000.

Yang, L. X., Wang, D. C., Cheng, S. H., Wang, Z., Zhou, Y., Zhou, X. H., and Wang, W. X.,: Influence of meteorological conditions and particulate matter on visual range impairment in Jinan, China, Sci. Total Environ., 383, 164–173, 2007.

Yang, L. X., Gao, X. M., Wang, X. F., Nie, W., Wang, J., Gao, R., Xu, P. J., Shou, Y. P., Zhang, Q. Z., and Wang, W. X.: Impacts of firecracker burning on aerosol chemical characteristics and human health risk levels during the Chinese New Year Celebration in Jinan, China, Sci. Total Environ., 476–477, 57–64, 2014.

Ye, C., Chen, R. S., and Young, C.: Nian: when Chinese mythology aff ects air pollution, Lancet, 383, 2125, doi:10.1016/S0140-6736(14)61029-1, 2014.

Yu, X. N., Shi, C. Z., Ma, J., Zhu, B., Li, M., Wang, J., Yang, S. Y., and Kang, N.: Aerosol optical properties during firework, biomass burning and dust episodes in Beijing, Atmos. Environ., 81, 475–484, 2013.

Zhang, M., Wang, X. M., Chen, J. M., Cheng, T. T., Wang, T., Yang, X., Gong, Y. G., Geng, F. H., and Chen, C. H.: Physical characterization of aerosol particles during the Chinese New Year's firework events, Atmos. Environ., 44, 5191–5198, 2010.

ACPD
14, 28609–28655, 2014

Table 1. Mass concentrations of elements in $PM_{2.5}$ before, during and after 2014 Chinese Spring Festival at Nanjing (ng m^{-3}).

Elements	Pre-SF	SF (without CNY)	After-SF (without LF)	CNY	LF	CNY/pre-CNY	LF/pre-LF
Li	1.9 ± 0.7	1.1 ± 0.8	1.4 ± 1.0	2.3	1.4	1.8	1.3
Be	0.1 ± 0.0	0.0 ± 0.0	0.0 ± 0.0	0.0	0.0	2.1	1.9
Na	826 ± 209	417 ± 196	435 ± 172	563	506	1.3	1.1
Mg	124 ± 79	97 ± 89	106 ± 30	196	124	2.6	1.3
Al	612 ± 234	802 ± 550	530 ± 230	3127	811	7.9	1.7
Si	1105 ± 420	752 ± 147	847 ± 422	1431	943	2.3	1.4
P	66 ± 35	35 ± 20	29 ± 13	42	35	1.5	1.3
K	1940 ± 725	3330 ± 3848	1276 ± 817	14 336	2940	9.3	1.8
Ca	454 ± 198	355 ± 95	383 ± 193	454	469	1.9	1.6
Sc	0.1 ± 0.0	0.1 ± 0.0	0.1 ± 0.1	0.1	0.1	1.5	1.4
Ti	31 ± 27	14 ± 8	24 ± 28	20	15	1.2	1.7
V	7.7 ± 2.3	7.0 ± 7.8	6.6 ± 4.6	9.4	10.5	1.2	2.4
Cr	10.4 ± 4.0	7.9 ± 5.7	8.7 ± 3.4	17.4	10.2	2.9	1.3
Mn	48 ± 22	22 ± 19	67 ± 67	47	50	1.9	1.3
Fe	385 ± 342	160 ± 140	261 ± 172	304	300	1.8	1.9
Co	0.4 ± 0.1	0.4 ± 0.4	0.4 ± 0.2	0.6	0.5	2.6	1.6
Ni	8.5 ± 6.0	4.5 ± 3.1	8.9 ± 5.6	5.9	7.6	1.3	1.5
Cu	102 ± 30	81 ± 63	77 ± 25	170	116	1.3	1.3
Zn	257 ± 145	93 ± 81	194 ± 154	242	174	1.6	1.3
As	17 ± 13	9.0 ± 9.8	8.0 ± 4.6	22	8.8	2.2	1.3
Rb	8.5 ± 2.2	4.7 ± 4.2	5.7 ± 4.5	12	6.5	1.7	1.5
Sr	5.1 ± 3.9	34 ± 49	4.9 ± 5.9	181	20.5	79.4	5.7
Y	0.2 ± 0.1	0.1 ± 0.1	0.2 ± 0.1	0.1	0.2	1.5	1.5
Zr	1.9 ± 0.7	1.6 ± 0.6	1.9 ± 1.3	1.6	2.3	1.2	1.4
Mo	2.7 ± 1.0	1.3 ± 1.2	2.9 ± 1.8	2.8	2.7	1.6	0.6
Cd	3.4 ± 2.8	1.3 ± 1.4	1.1 ± 0.7	4.1	1.3	1.7	1.3
Sn	9.0 ± 5.6	5.0 ± 6.1	4.6 ± 3.5	18.0	4.5	3.7	1.1
Sb	11 ± 6.5	4.8 ± 5.4	3.0 ± 1.6	13.9	4.8	2.9	1.7
Cs	1.8 ± 1.0	0.7 ± 0.8	1.4 ± 1.5	1.9	1.2	1.4	1.4
Ba	14 ± 12	152 ± 216	14.4 ± 20.4	850	70.1	99.1	9.7
La	0.7 ± 0.6	0.6 ± 0.5	0.6 ± 0.5	0.6	0.5	2.5	0.8
Ce	0.8 ± 0.5	0.4 ± 0.3	0.6 ± 0.6	0.6	0.5	2.3	1.0
Sm	0.1 ± 0.0	0.0 ± 0.0	0.0 ± 0.0	0.0	0.0	1.4	1.2
W	4.3 ± 2.4	3.1 ± 2.9	3.2 ± 1.3	4.7	5.4	0.6	1.1
Tl	1.4 ± 0.7	0.5 ± 0.5	0.8 ± 0.5	1.4	0.8	1.4	1.2
Pb	187 ± 96	116 ± 132	91 ± 54	425	127	2.6	1.0
Bi	7.3 ± 5.4	9.1 ± 13.0	3.0 ± 2.2	36.9	6.5	7.2	2.3
Th	0.6 ± 0.0	0.5 ± 0.0	0.6 ± 0.0	0.6	0.6	1.0	1.0
U	0.1 ± 0.0	0.0 ± 0.0	0.1 ± 0.1	0.1	0.1	1.4	1.2

Pre-SF indicated the period before 2014 Chinese Spring Festival (SF), covering the days from 24 to 29 January; SF indicated the Spring Festival period, covering the days from 30 January to 6 February; After-SF indicated the period after Spring Festival, covering the days from 12 to 21 February. CNY indicates the Chinese New Year (CNY) day and in 2014, it is 30 January; pre-CNY is the day before CNY and is 29 January. LF indicates the Lantern Festival (LF) day and in 2014, it is 14 February; pre-LF is the day before LF and is 14 Febraury. At CNY and LF, intensive fireworks were burned. Therefore, the mass concentrations of $PM_{2.5}$ and associated chemical species of the two days were listed seperately. CNY/pre-CNY indicates the ratios between mass concentrations of $PM_{2.5}$ and associated chemical species at CNY and the day before CNY (pre-CNY). LF/pre-LF indicates the ratios between mass concentrations of $PM_{2.5}$ and associated chemical species at LF and the day before LF (pre-LF).

ACPD
14, 28609–28655, 2014

Table 2. Mass concentrations of ions and carbonaceous species in $PM_{2.5}$ before, during and after 2014 Chinese Spring Festival at Nanjing ($\mu g\,m^{-3}$).

Elements	Pre-SF	SF (without CNY)	After-SF (without LF)	CNY	LF	CNY/pre-CNY	LF/pre-LF
Na^+	0.65 ± 0.17	0.37 ± 0.07	0.31 ± 0.09	0.40	0.29	0.7	1.0
NH_4^+	4.26 ± 1.12	4.81 ± 3.68	5.33 ± 1.98	10.5	6.85	2.4	1.3
K^+	0.49 ± 0.31	1.59 ± 1.55	0.67 ± 0.22	4.81	1.06	8.9	1.8
Ca^{2+}	0.09 ± 0.05	0.23 ± 0.14	0.19 ± 0.09	0.25	0.18	3.3	0.8
Mg^{2+}	0.03 ± 0.03	0.20 ± 0.31	0.08 ± 0.04	0.10	0.09	1.3	1.5
F^-	0.03 ± 0.01	0.04 ± 0.02	0.03 ± 0.01	0.05	0.04	2.2	1.4
Cl^-	1.16 ± 0.26	0.72 ± 0.54	0.75 ± 0.40	3.04	1.09	3.8	1.2
NO_2^-	0.02 ± 0.01	0.04 ± 0.01	0.04 ± 0.01	0.02	0.05	0.8	1.7
NO_3^-	5.81 ± 2.54	5.27 ± 5.38	6.59 ± 2.98	14.6	8.36	2.5	1.3
SO_4^{2-}	3.46 ± 1.28	7.74 ± 5.17	4.05 ± 2.34	16.1	4.54	4.4	1.1
OC	18.2 ± 7.45	9.38 ± 6.70	8.95 ± 3.15	56.9	12.2	4.1	1.1
EC	6.93 ± 4.64	3.12 ± 3.06	2.96 ± 1.20	8.29	3.38	1.8	0.9
OC1	1.87 ± 1.40	0.40 ± 0.23	0.50 ± 0.16	16.1	0.64	33.2	1.1
OC2	4.32 ± 1.65	2.56 ± 1.75	2.36 ± 0.74	14.8	2.86	4.2	1.1
OC3	5.46 ± 2.69	2.77 ± 2.09	2.90 ± 1.15	9.10	4.28	2.4	1.0
OC4	5.44 ± 1.52	3.27 ± 3.03	2.94 ± 1.36	5.81	4.46	0.9	1.1
EC1	7.92 ± 5.07	3.44 ± 2.64	3.15 ± 1.00	18.8	3.30	4.1	0.9
EC2	0.12 ± 0.07	0.07 ± 0.06	0.06 ± 0.05	0.50	0.08	37.7	1.6
EC3	0.00 ± 0.00	0.00 ± 0.00	0.00 ± 0.00	0.11	0.00	–	–
OPC	1.12 ± 2.43	0.39 ± 0.39	0.24 ± 0.43	11.09	0.00	–	–
$PM_{2.5}$	119.6 ± 43.4	106.9 ± 84.1	88.9 ± 37.4	318.0	118.4	3.1	1.3

– Not detected in the day before CNY and LF.
Pre-SF indicated the period before 2014 Chinese Spring Festival (SF), covering the days from 24 to 29 January; SF indicated the Spring Festival period, covering the days from 30 January to 6 February; After-SF indicated the period after Spring Festival, covering the days from 12 to 21 February. CNY indicates the Chinese New Year (CNY) day and in 2014, it is 30 January; pre-CNY is the day before CNY and is 29 January. LF indicates the Lantern Festival (LF) day and in 2014, it is 14 February; pre-LF is the day before LF and is 14 February. At CNY and LF, intensive fireworks were burned. Therefore, the mass concentrations of $PM_{2.5}$ and associated chemical species of the two days were listed seperately. CNY/pre-CNY indicates the ratios between mass concentrations of $PM_{2.5}$ and associated chemical species at CNY and the day before CNY (pre-CNY). LF/pre-LF indicates the ratios between mass concentrations of $PM_{2.5}$ and associated chemical species at LF and the day before LF (pre-LF).

ACPD
14, 28609–28655, 2014

Table A1. Abbreviations glossary.

Fireworks burning	FW
Chinese New Year day	CNY
Spring Festival	SF
Lantern Festival	LF
Organic carbon	OC
Elemental carbon	EC
Black carbon	BC
Organic matter	OM
Relative humidity	RH
Inductively coupled plasma-mass spectroscopy	ICP-MS
Inductively coupled plasma-optical emission spectrometer	ICP-OES
Optically detected pyrolized carbon	OPC
Principal component analysis	PCA
Lifetime average daily dose	LADD
Inhalation rate	InhR
Exposure frequency	EF
Exposure duration	ED
Average body weight	BW
Averaging time	AT
Hazard Quotient	HQ
Reference dose	RfD
Hazard Index	HI
Mineral matter	MIN
Trace elements	TE
Sea salt	SS
Secondary inorganic aerosol	SIA
Unidentified matter	UM
Correlation coefficient	R^2
Weather Research and Forecast model	WRF
The day before CNY	Pre-CNY
The day before LF	Pre-LF
The period before Spring Festival	Pre-SF
The period after Spring Festival	After-SF
Mass calculated by adding individual components	PM_{cal}
Gravimetrically measured particulate mass	PM_{meas}
Visibility calculated by adding individual components	V_{cal}
Measured visibility	V_{meas}
Extinction coefficient	b_{ext}
Local time	LT

ACPD
14, 28609–28655, 2014

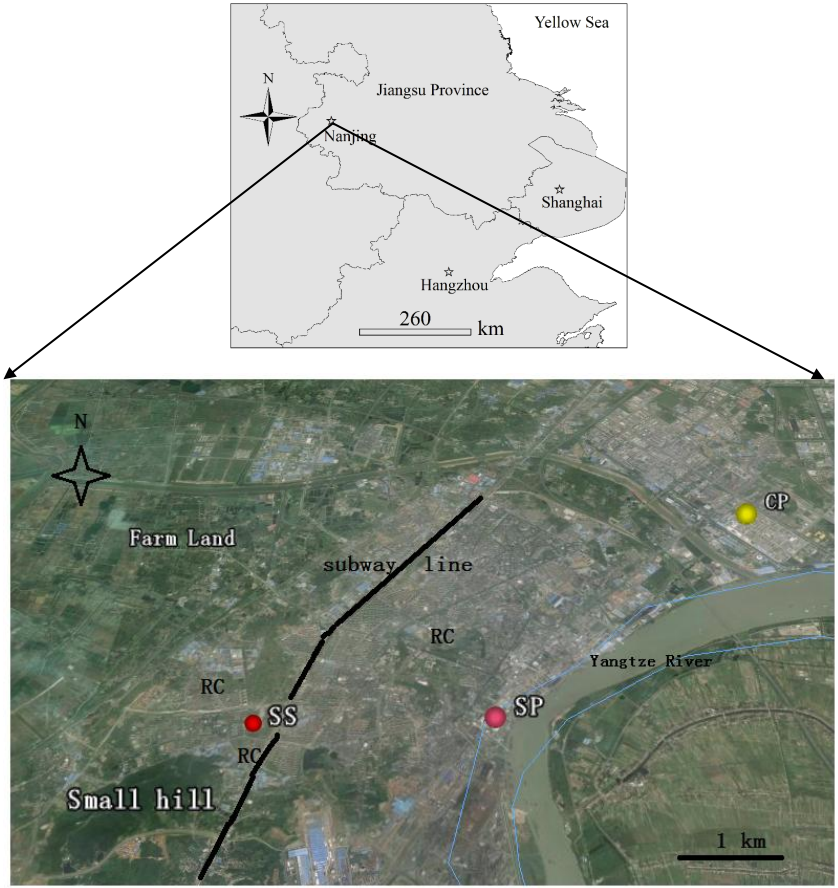

Figure 1. Location of the sampling site (the red dot, SS). SP: iron smelt plant; CP: chemical industrial park; RC: residential community. The black line indicates the subway line near SS.

ACPD
14, 28609–28655, 2014

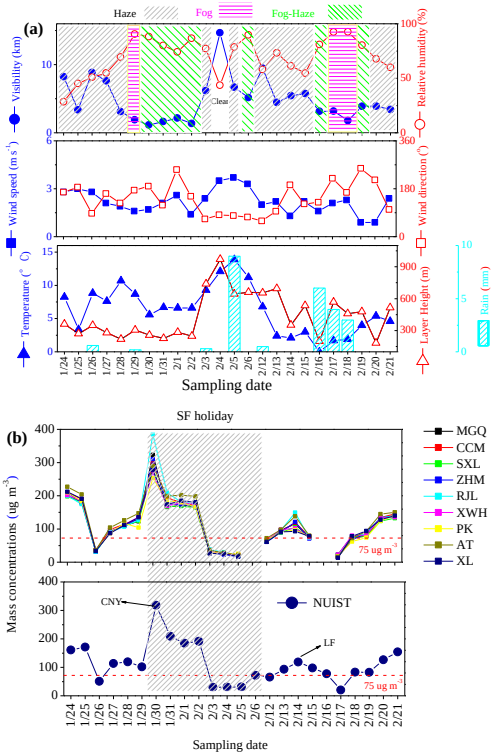

Figure 2. Daily variation of meteorological factors **(a)** and mass concentrations of $PM_{2.5}$ **(b)** during sampling periods. MGQ, CCM, SXL, ZHM, RJL, XWH, PK, AT and XL indicate the nine urban air quality monitoring sites set by Jiangsu Environmental Monitoring Center as Supplement S4 shown. NUIST indicates the sampling site of this study at Nanjing University of Information Science and Technology. SF means Spring Festival (between 30 January–7 February); CNY means Chinese New Year day (at 30 January); LF means Lantern Festival day (at 14 February). 75 μm^{-3} is the 24 h-averaged secondary standard for $PM_{2.5}$ of China National Ambient Air Quality.

ACPD
14, 28609–28655, 2014

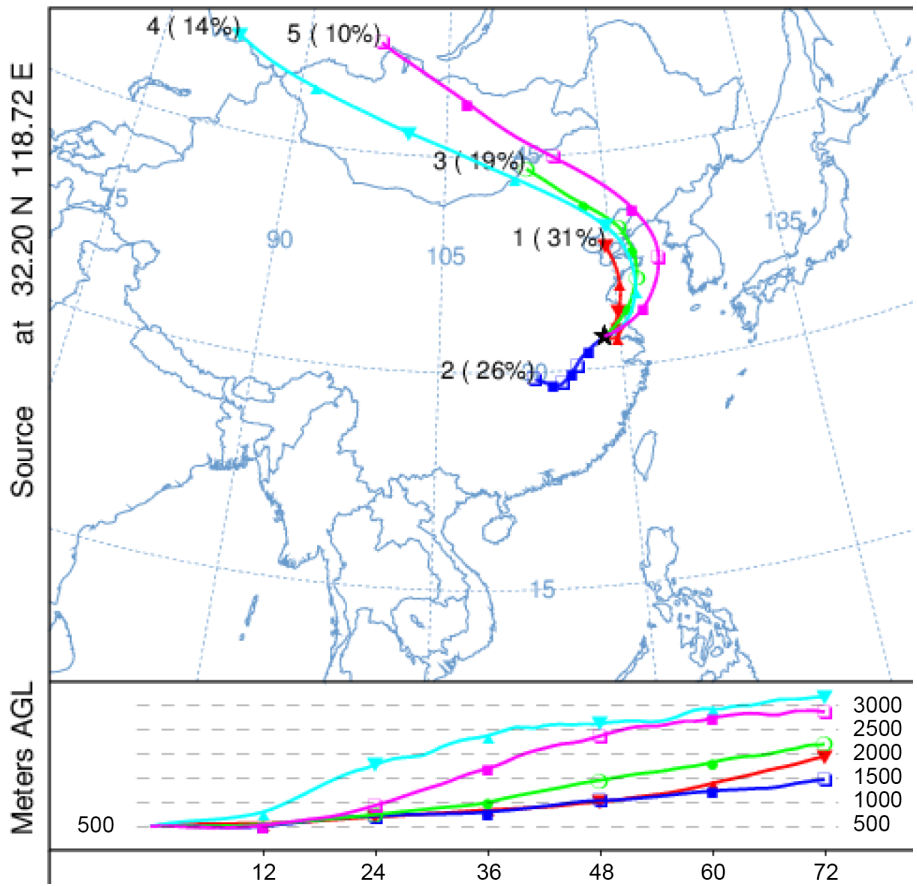

Figure 3. Cluster analysis for backward trajectories of air masses during the whole sampling periods. The different colors indicated different clusters of the backward trajectories.

ACPD
14, 28609–28655, 2014

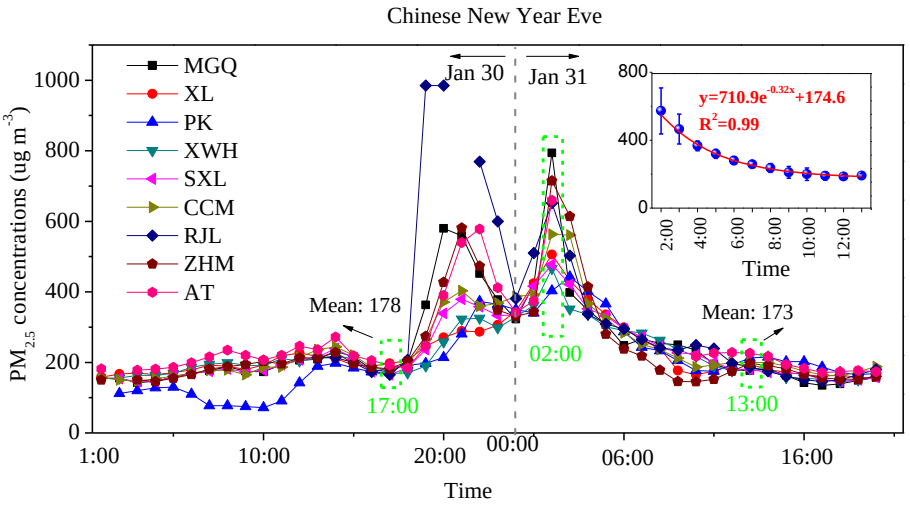

Figure 4. Hourly $PM_{2.5}$ concentrations before, during and after Chinese New Year (CNY)'s Eve of 2014 at Nanjing. The figure at the top-right corner indicates the decreasing trend of averaged $PM_{2.5}$ mass concentrations after 02:00 LT of CNY's Eve (at 30 January 2014). Hourly data for the nine sites in urban Nanjing (locations were shown in Supplement S4) were collected from the public platform at http://218.94.78.75/jsair/.

ACPD
14, 28609–28655, 2014

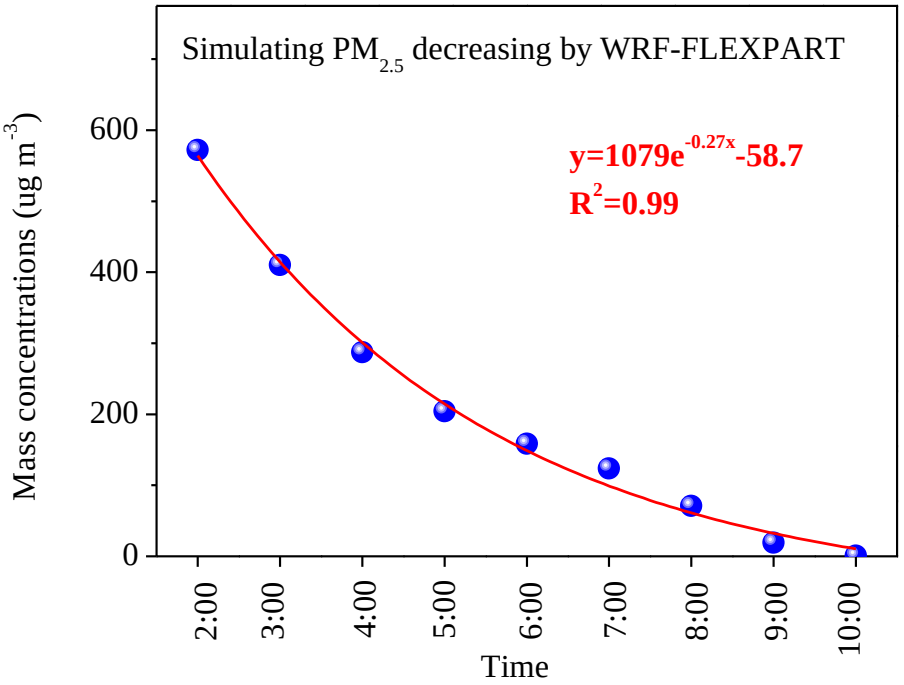

Figure 5. Particles decreasing trend at Chinese New Year's Eve by WRF-FLEXPART simulating. The particle concentrations decreased to 0.76 $\mu g\,m^{-3}$ after nine hours, faster than the real decrease as Fig. 4 shows. It can be explained as that we did not consider the injections of particles during simulating course, which biases the result.

ACPD
14, 28609–28655, 2014

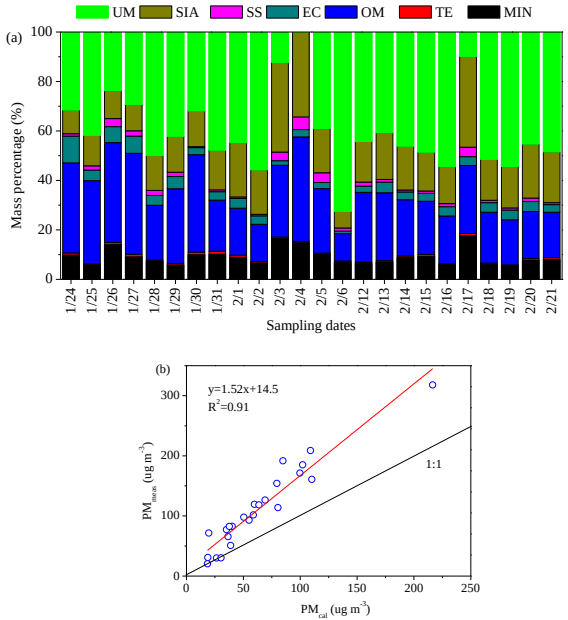

Figure 6. Mass balance of chemical species in $PM_{2.5}$ at sampling periods **(a)** and relationship between the mass calculated by adding individual components and the gravimetrically measured particulate mass **(b)**. MIN = 2.14 × Si + 1.67 × Ti + 1.89 × Al + 1.59 × Mn + 1.67 × Mg + 1.95 × Ca + 1.35 × Na + 1.21 × K + 1.43 × Fe. Trace elements (TE) indicated the sum of all other elements except for those used in calculating MIN. Sea salt (SS) = $[Na^+]$ + $[ss\text{-}Cl^-]$ + $[ss\text{-}Mg^{2+}]$ + $[ss\text{-}K^-]$ + $[ss\text{-}Ca^{2+}]$ + $[ss\text{-}SO_4^{2-}]$; $ss\text{-}Cl^- = 1.8 \times [Na^+]$; $ss\text{-}Mg^{2+} = 0.12 \times [Na^+]$; $ss\text{-}K^- = 0.036 \times [Na^+]$; $ss\text{-}Ca^{2+} = 0.038 \times [Na^+]$; $ss\text{-}SO_4^{2-} = 0.252 \times [Na^+]$. Secondary inorganic aerosol (SIA) was calculated as the sum of $nss\text{-}SO_4^{2-}$, NO_3^- and NH_4^+. Organic matter (OM) = 2.0 × OC. UM indicated unidentified matter. 30 January–7 February belongs to the Chinese Spring Festival in 2014; 30 January is the Chinese New Year day; 14 February is the Lantern Festival day.

ACPD
14, 28609–28655, 2014

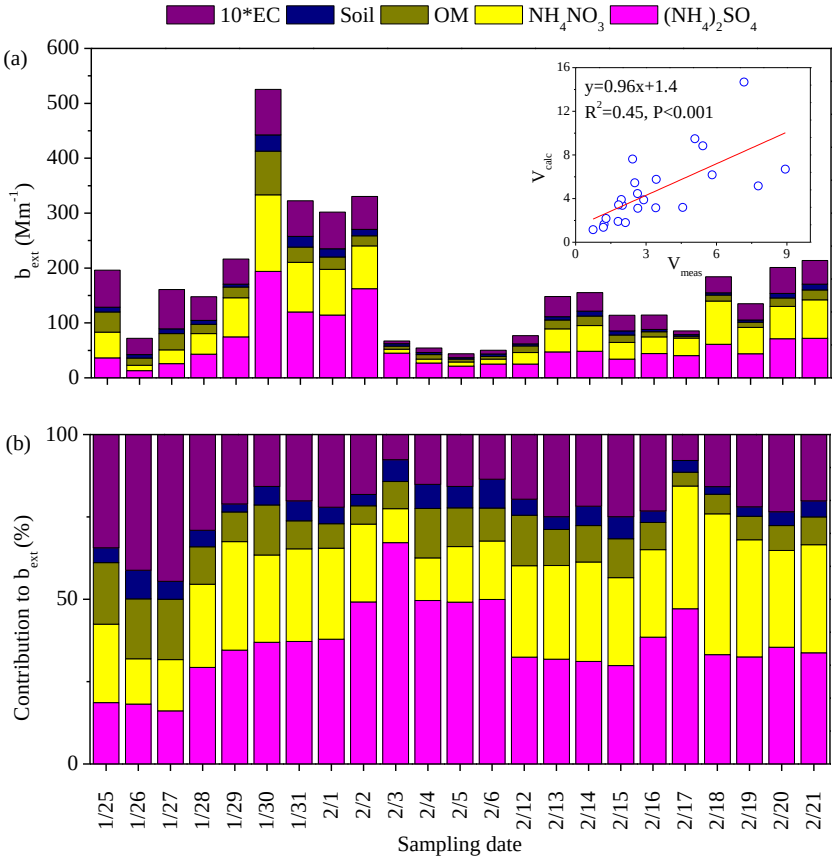

Figure 7. Extinction coefficients of chemical components in $PM_{2.5}$ at Nanjing **(a)** and relative contribution to light extinction of chemical components in $PM_{2.5}$ **(b)**. 30 January–7 February belongs to the Chinese Spring Festival in 2014; 30 January is the Chinese New Year day; 14 February is the Lantern Festival day. V_{cal} indicates the visibility calculated by adding individual components; V_{meas} is the measured visibility.

ACPD
14, 28609–28655, 2014

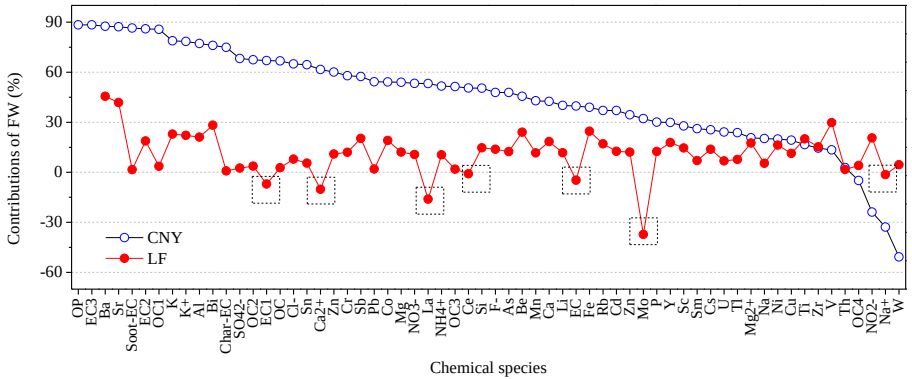

Figure 8. Contributions of fireworks burning (FW) at CNY and LF to chemical species in $PM_{2.5}$. CNY means Chinese New Year day (30 January); LF means Lantern Festival day (14 February).

ACPD
14, 28609–28655, 2014

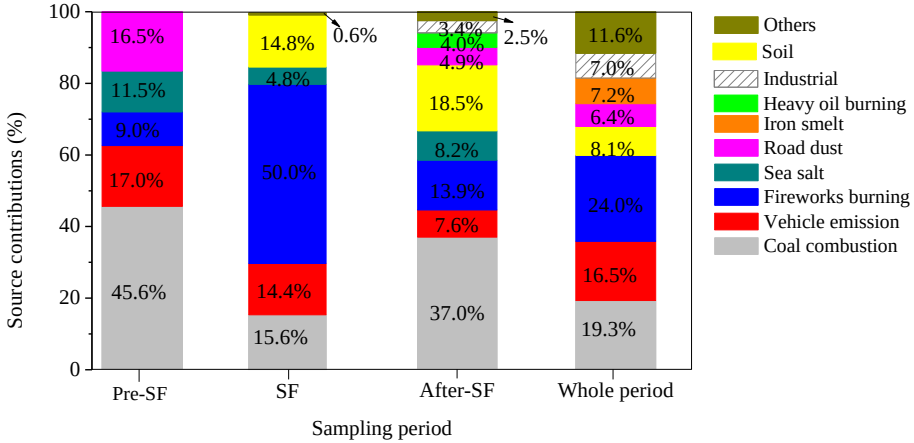

Figure 9. Source contributions to atmospheric $PM_{2.5}$ before, during, after 2014 Spring Festival (SF) and the whole period by principal component analysis. Pre-SF indicated the period before SF, covering the days from 24 to 29 January; SF indicated the period during SF, covering the days from 30 January to 6 February; After-SF indicated the period after SF, covering the days from 12 to 21 February.

ACPD
14, 28609–28655, 2014

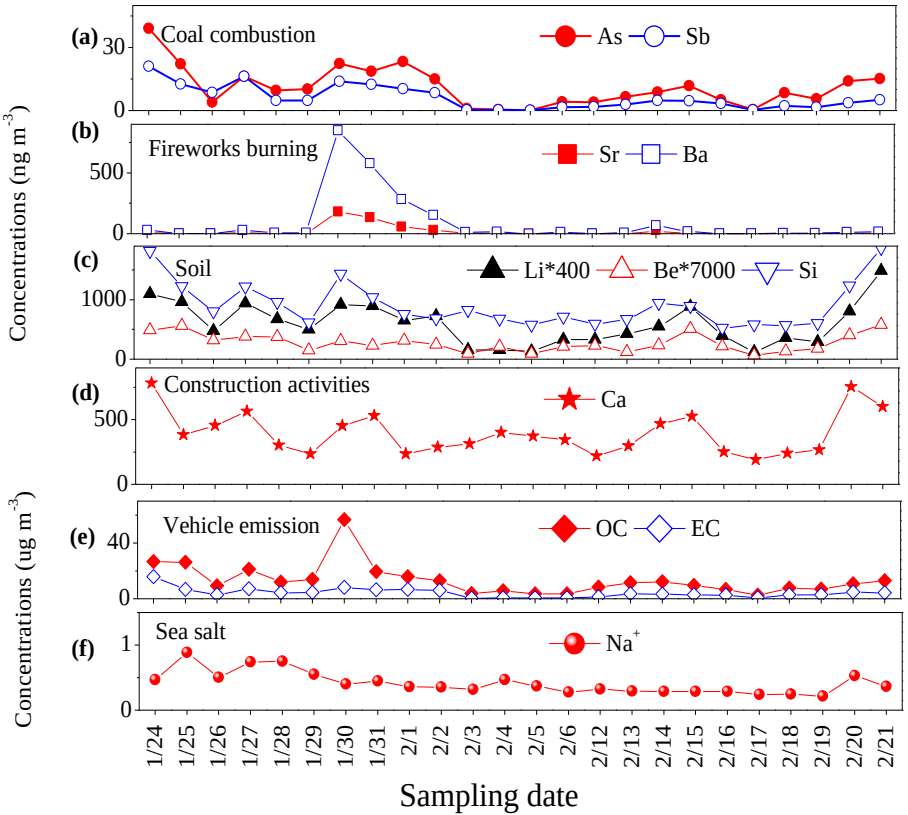

Figure 10. Time series of tracers for **(a)** coal combustion, **(b)** fireworks burning, **(c)** soil, **(d)** construction activities or road dust, **(e)** vehicle emission and **(f)** sea salt. The *y* axis units for **(a–d)** are ng m^{-3} and are ug m^{-3} for (**e** and **f**). 30 January–7 February belongs to the Chinese Spring Festival in 2014; 30 January is the Chinese New Year day; 14 February is the Lantern Festival day.

ACPD
14, 28609–28655, 2014

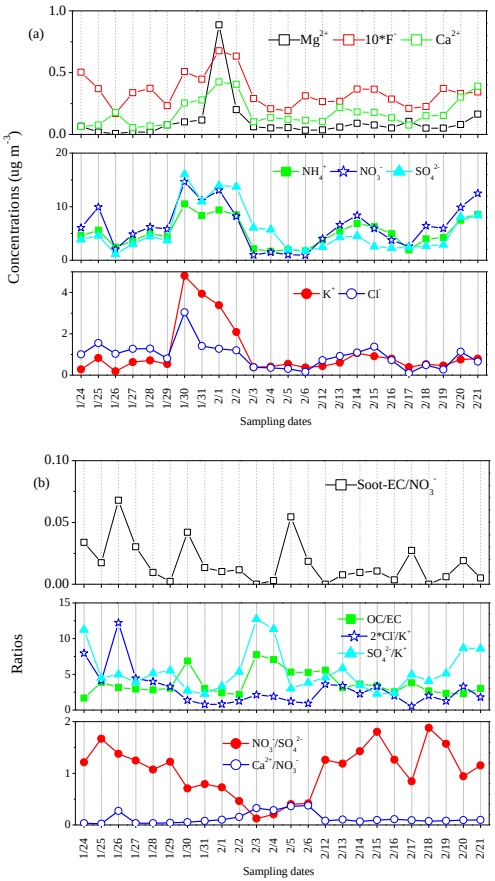

Figure 11. Time series of ions **(a)** and specific ratios **(b)** during sampling period. 30 January–7 February belongs to the Chinese Spring Festival in 2014; 30 January is the Chinese New Year day; 14 February is the Lantern Festival day.

ACPD
14, 28609–28655, 2014

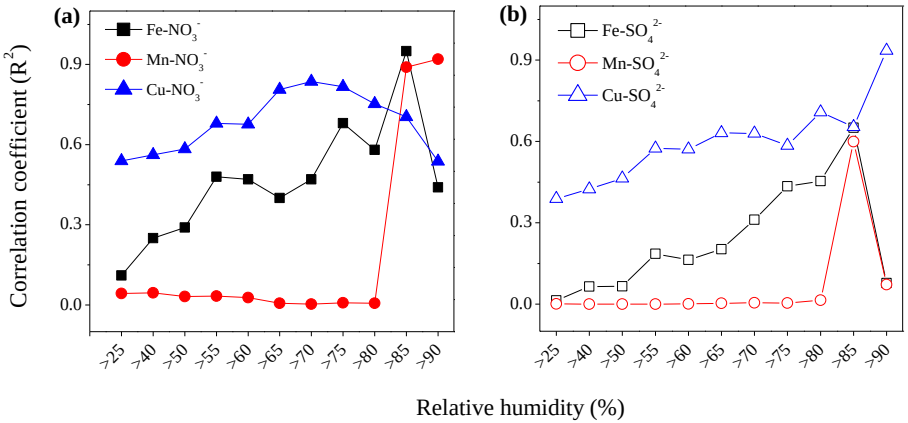

Figure 12. Correlation coefficients (R^2) of NO_3^- and metals-Fe, Mn and Cu under certain relative humidity bins **(a)**; correlation coefficients of SO_4^{2-} and metals-Fe, Mn and Cu under certain relative humidity bins **(b)**. For each time of calculating the R^2, the data of NO_3^- or SO_4^{2-} and each metal were used for corresponding relative humidity bins.

ACPD
14, 28609–28655, 2014

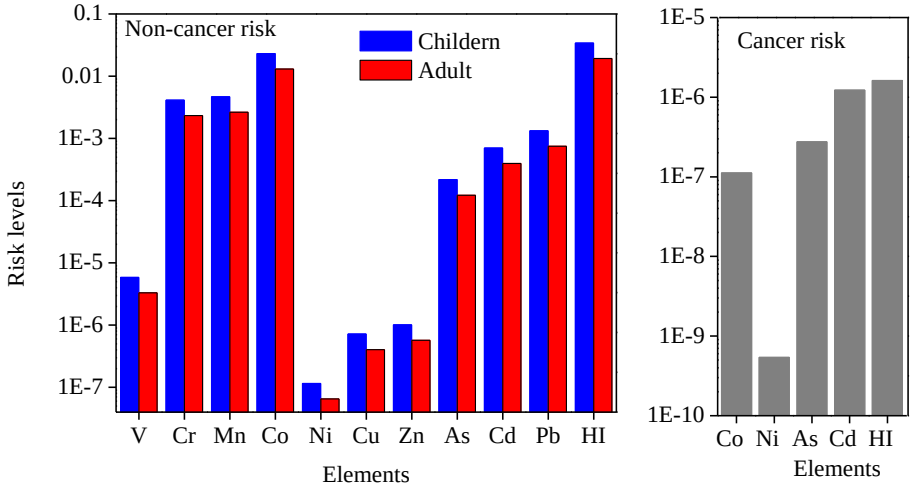

Figure 13. Non-cancer and cancer risks for heavy metals raised by intensive fireworks burning at Nanjing.

ACPD
14, 28609–28655, 2014